

*Review*

## Microwave Plasma Synthesis of Materials—From Physics and Chemistry to Nanoparticles: A Materials Scientist's Viewpoint

Dorothee Vinga Szabó \* and Sabine Schlabach

Karlsruhe Institute of Technology, Institute for Applied Materials, Hermann-von-Helmholtz-Platz 1, 76344 Eggenstein-Leopoldshafen, Germany; E-Mail: sabine.schlabach@kit.edu

\* Author to whom correspondence should be addressed; E-Mail: dorothee.szabo@kit.edu; Tel.: +49-721-608 (ext. 22938); Fax: +49-721-608 (ext. 23956).

*Received: 10 June 2014; in revised form: 6 August 2014 / Accepted: 11 August 2014 /*

*Published: 18 August 2014*

---

**Abstract:** In this review, microwave plasma gas-phase synthesis of inorganic materials and material groups is discussed from the application-oriented perspective of a materials scientist: why and how microwave plasmas are applied for the synthesis of materials? First, key players in this research field will be identified, and a brief overview on publication history on this topic is given. The fundamental basics, necessary to understand the processes ongoing in particle synthesis—one of the main applications of microwave plasma processes—and the influence of the relevant experimental parameters on the resulting particles and their properties will be addressed. The benefit of using microwave plasma instead of conventional gas phase processes with respect to chemical reactivity and crystallite nucleation will be reviewed. The criteria, how to choose an appropriate precursor to synthesize a specific material with an intended application is discussed. A tabular overview on all type of materials synthesized in microwave plasmas and other plasma methods will be given, including relevant citations. Finally, property examples of three groups of nanomaterials synthesized with microwave plasma methods, bare Fe<sub>2</sub>O<sub>3</sub> nanoparticles, different core/shell ceramic/organic shell nanoparticles, and Sn-based nanocomposites, will be described exemplarily, comprising perspectives of applications.

**Keywords:** microwave plasma; gas-phase synthesis; chemical reactions; material; nanoparticles

---

## 1. Introduction

Since the end of the late 1980s, several gas phase synthesis methods are used for the synthesis of materials, especially matter in form of powders and nanoparticles [1–12]. The common feature of all gas phase methods is that they use vaporized chemical compounds or precursors, which undergo a chemical reaction in a gaseous environment. The evaporated individual atoms or molecules collide, and particle formation is starting by a homogeneous nucleation process. The nuclei grow by condensation of vapor molecules on already existing particles. Nucleation and coalescence processes are well described and understood for standard gas-phase reactions and aerosol processes [13–15]. By ongoing collisions of particles and by coagulation the particles grow further. Energy supply for the desired reactions may be either thermal (high temperature, flame, laser), or by a plasma (microwave (MW), radio-frequency (RF), dielectric barrier discharge (DBD), alternating current (AC), direct current (DC), induction, or electric arc (EA)).

Several research groups worldwide apply microwave plasma processes for the synthesis of particulate matter, mainly. The advantage of using microwave energy is, that higher degrees of ionization and dissociation can be obtained, compared to other types of electrical excitation [16]. This higher ionization and dissociation reduces the activation energy and enhances the kinetics to initiate a chemical reaction. Furthermore, lower temperatures can be realized in comparison to thermal plasmas or standard thermal reactions, being favorable for yielding in smaller particles. Although the focus of this article is “microwave plasma”, many statements or comparison will be done with “RF plasma”, as the basis of theoretical papers in this field is much broader than in the field of “microwave plasma”.

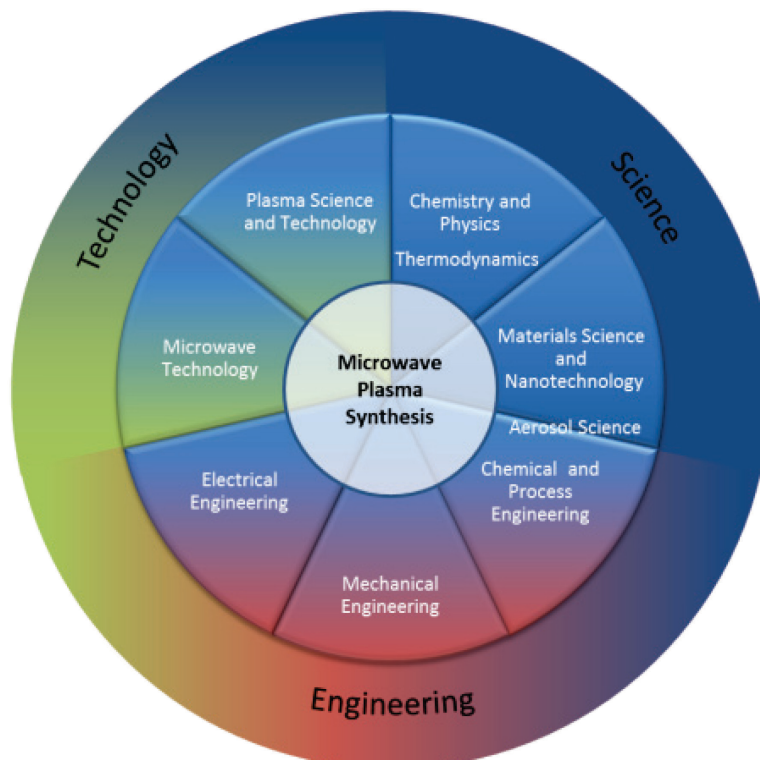
This feature article will focus on the application of microwave plasmas for the synthesis of nanoparticles in the gas-phase from the viewpoint of a materials scientist, using a physical method to synthesize materials with particle-size dependent properties. Other applications of microwave plasma methods, frequently described in literature, are etching and coating of surfaces, and the synthesis of tubes, wires, or rods. The topic of gas phase reactions in microwave plasma is an interdisciplinary field of science, engineering, and technology, interplaying with microwave technology, as well as plasma science and technology, chemistry, physics, nanotechnology, and materials science. It also refers to topics of electrical engineering, chemical and process engineering, and mechanical engineering. Thermodynamics and aerosol science are further disciplines in touch with the subject. These interconnected relationships are shown schematically in Figure 1.

## 2. Definition of Terms

Before starting in detail the discussions on different subjects, the relevant terms used in this article are shortly explained in the context they are applied.

- **Microwaves** are electromagnetic waves in the frequency range from 300 GHz to 300 MHz. The corresponding wavelengths range from 1 mm to 1 m. Industrially used microwave frequencies are 0.915 GHz with wavelength  $\lambda \sim 32$  cm (mobile phone, food processing), and 2.45 GHz with  $\lambda \sim 12$  cm (kitchen microwave, microwave sterilization).

**Figure 1.** Interlinked research activities between microwave plasma synthesis and the contributing scientific, technological and engineering disciplines.



- In physics and chemistry, **plasma** is typically an ionized gas [17]. It contains neutral as well as charged elementary particles (electrons, ions, molecules). Plasma is considered to be a distinct state of matter because of its unique properties. The term “ionized” refers to the presence of one or more free electrons, which are not bound to an atom or molecule. The free electric charges make the plasma electrically conductive so that it responds strongly to electromagnetic fields.
- Plasma, containing particles (in the sense of particulate matter), is called “**dusty plasma**”. This type of plasma is used for particles syntheses [18]. In the context of this paper, “particle” has the meaning of particulate matter.
- **Thermal plasmas** are characterized by a thermodynamic equilibrium, meaning that all species (electrons, ions, and neutral species) have the same temperature (energy). An example for thermal plasma is arc plasma. Its temperature may be around 10,000 K. This type of plasma is mainly not part of this article.
- **Non-thermal plasmas** are characterized by a thermal **non-equilibrium** between the temperature of the electrons and the ions. The temperature of the electrons ranges between several electron volt (eV), whereas the temperature of the positively charged ions and neutral species is significantly colder (around room temperature) [19,20], leading to a quite low overall temperature. Therefore, non-thermal plasmas, also called non-equilibrium plasmas, are favorable for the synthesis of nanoparticles at low temperatures. They can be ignited by microwaves, but also by, e.g., RF or by DBD [9,21]. The temperature of the plasma is around 300–1000 K. Therefore, this type of plasma is also called “cold plasma”.

- **Atmospheric pressure plasmas** are operated at atmospheric pressure. They are favorable for industrial processes, as they need smaller experimental efforts and thus lower costs. Ignition is possible by DC, by RF, and by microwaves. Atmospheric plasmas may be thermal plasmas or non-thermal plasmas [22].
- **Low-pressure plasmas** are operated under vacuum conditions (several 100 Pa to 10,000 Pa). They require more expensive vacuum-components and more sophisticated set-ups. They are usually “cold plasmas”.
- **Nanomaterials**, respectively **nanoparticles**, are particulate matter and generally defined as materials with grain sizes below 100 nm in at least one dimension. A more stringent definition is to specify nanomaterials or nanoparticles as materials with particles size dependent properties.
- **Gas-phase processes** are chemical reactions, where gaseous components react in a gaseous environment to form solid reaction products (e.g., particles). All plasma reactions in the context of this paper are gas-phase reactions.

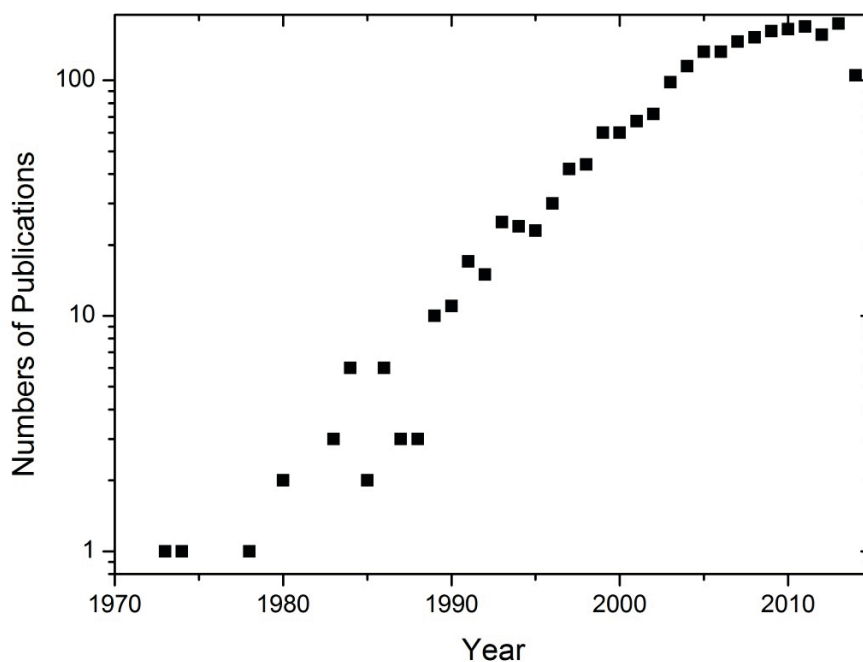
### 3. Microwave Plasma Processes for Materials Synthesis in Literature

In the first part of this article, a dedicated literature search using “Scopus” will be presented. This search is applied to identify the key players in the field of microwave plasma synthesis of materials. In the second part, a short historical overview will be given, showing the development of the topic by the years.

#### 3.1. Finding the Key Players

The key players were identified based on a search using “Scopus” (www.scopus.com, last update of the queries on 30 July 2014). The starting query uses the key-words “nonthermal\*”, “non-thermal\*”, “microwave\*”, “low pressure\*”, or “non-equilibrium”, combined with “plasma\*”. The terms “Life Sciences”, “Health Sciences”, and “Social Sciences and Humanities” are categorically excluded. The starting key words yield in 50,952 hits. Thereafter, the search was refined, adding and combining other related key words (“nano\*”, “material\*”, “synthes\*”, “particl\*”, and “gas phase”), yielding in 2234 hits. The number of papers published per year (refined results) is shown in Figure 2. This figure also contains the hits of groups working with microwave plasma enhanced chemical vapor deposition (CVD), sintering, etching, or on nanotubes, nanowires or thin film synthesis using microwave plasma. In addition, non-thermal plasmas generated with radio frequency are part of the results.

The outstanding key players in the field of microwave plasma gas-phase synthesis of particulate matter are identified as University of Minnesota, Twin Cities (MN, USA), Karlsruhe Institute of Technology (Germany), Pennsylvania State University (PA, USA), University of Duisburg-Essen (Germany), Ajou University, (Korea), Los Alamos National Laboratory (NM, USA), ITRI—Industrial Technology Research Institute, (Taiwan), and Academy of Sciences of the Czech Republic/Masaryk University, Brno (Czech Republic). Beyond these key groups, also research results from less common groups are found in literature.

**Figure 2.** Number of papers published per year.

### 3.2. Microwave Plasma Synthesis of Particulate Matter in the Historical Context

In 1973, Bosisio *et al.* already describe the attractiveness of microwave plasma in the field of chemistry and spectroscopy [16], as higher degrees of ionization and dissociation can be achieved in comparison to other types of electrical excitation. In that decade, microwave plasmas have been mainly applied for cleaning or etching silicon substrates in semiconducting industry [23–26]. In this context, the particle formation was considered as a contamination problem of “dusty” plasmas, before the potential of “dusty” plasma for particle synthesis was recognized. An overview on plasma processing of materials is presented by Szekeley in 1984 [27], distinguishing between thermal plasmas and non-equilibrium plasmas. Synthesis of particulate matter is not a topic of this paper. Several review papers in the mid-1980s present fundamental background aspects of plasmas generated by other energy sources than microwaves [28,29] and on chemical reactions and nucleation in thermal plasmas [30,31]. Moisan and Wertheimer [32] reviewed, in 1993, the excitation frequency effects in plasma processes. They present experimental evidence which confirms theoretical predictions that microwave plasmas are generally more efficient than their RF counterparts.

Diamond synthesis using a microwave plasma was reported by Kamo *et al.* [33] in 1983, and by Saito *et al.* [34,35] in 1986 and 1988. Takagi *et al.*'s [36] report in 1990 was on quantum size effects of ultrafine Si particles they made in a microwave plasma. The first conference papers on ceramic particle synthesis in microwave plasmas were published by Metha *et al.* in 1991 [37], reporting on TiN and TiO<sub>2</sub> particles synthesized in a 2.45 GHz plasma. In 1992, Sickafus *et al.* [38] and Vollath *et al.* [39] reported on ZrO<sub>2</sub> and Al<sub>2</sub>O<sub>3</sub> nanoparticles, synthesized in a 0.915 GHz microwave plasma. The first scientific papers were published in 1992 by Chou *et al.* [40], regarding the synthesis of metallic Fe nanoparticles as well as Fe<sub>2</sub>O<sub>3</sub> nanoparticles in a 2.45 GHz plasma, and by Vollath and Sickafus [41] on the synthesis of Al<sub>2</sub>O<sub>3</sub>, ZrO<sub>2</sub>, and TiO<sub>2</sub> nanoparticles in a 0.915 GHz plasma. In 1993, Vollath and Sickafus [42,43] published the synthesis of ceramic nanoparticles in a 0.915 GHz microwave plasma. The

first ceramic core/shell particles, synthesized in two consecutive plasma zones were published in 1994 by Vollath and Szabó [44]. In 1997, Brenner *et al.* [45] synthesized nanoparticulate matter by decomposition of metal carbonyls in a 2.45 GHz Ar plasma. The dissolution of the carbonyls in toluene yielded in a carbonaceous support, produced simultaneously with the metal particles containing Fe, Co, and Co + Mo.

Whereas in the beginning of research activity in this field mainly feasibility of all kind of materials was in the focus of research, later on also theoretical considerations on microwave plasmas combined with a deeper understanding of the processes occurring in the plasma, and the interaction between different species in the plasma were of interest in the several groups [46–50]. Finally, in the last decade the properties and the application potential of the resulting materials have increased very much in interest [20,51–60].

#### 4. Physical Background of the Microwave Plasma Process and Technical Equipment

A great variety of plasma processes exists, but their classification in literature is sometimes confusing. They can be classified according to several criteria:

- operating pressure
  - low pressure plasma
  - atmospheric pressure plasma
- thermodynamic equilibrium
  - thermal or equilibrium plasma ( $T_{\text{electron}} \approx T_{\text{ion}} \approx T_{\text{gas}}$ )
  - non-thermal plasma or non-equilibrium plasma ( $T_{\text{electron}} \gg T_{\text{ion}} \approx T_{\text{gas}}$ )
- temperature
  - low temperature plasma ( $T_{\text{gas}} < 2000 \text{ K}$ )
  - high temperature plasma ( $T_{\text{gas}} > 2000 \text{ K}$ ).
- plasma generation
  - microwave discharge ( $300 \text{ MHz} \leq f \leq 300 \text{ GHz}$ )
  - radio frequency discharge (450 kHz–3.0 MHz; 13.56 MHz)
  - DC discharge
  - dielectric barrier discharge
  - corona discharge
  - electric arc
  - hollow cathode discharge
  - electron beam
  - plasma torch
  - alternating current
- type of coupling
  - inductive coupling
  - capacitive coupling

Numerous reviews on the topic of plasma are published by several authors and research groups, treating all facets of plasma synthesis methods and their applications: Vollath on plasma methods for the

synthesis of nanoparticles [9], Young and Pfender [28] and Ishigaki [61] on particles in thermal plasmas, Schütze *et al.* on atmospheric plasma jet [62], Tendero *et al.* on atmospheric pressure plasmas [22], Kortshagen [20] on non-thermal plasmas, Philips *et al.* on aerosol through plasma methods [63], Bárdos and Baránková [64] on cold atmospheric plasmas, Belmonte *et al.* [65] on non-equilibrium plasmas at atmospheric pressure, and Seiji *et al.* on the so-called “Plasma Roadmap” [18]. These reviews show that non-thermal plasmas can be generated by RF, or by microwaves. The non-thermal plasmas usually are operated as low pressure plasmas. The utilization of microwave plasmas at atmospheric pressure is also described. Additionally, microwave thermal plasmas are also in use. The application of microwaves for gas phase synthesis therefore covers the fields of low pressure, atmospheric, as well as thermal plasmas.

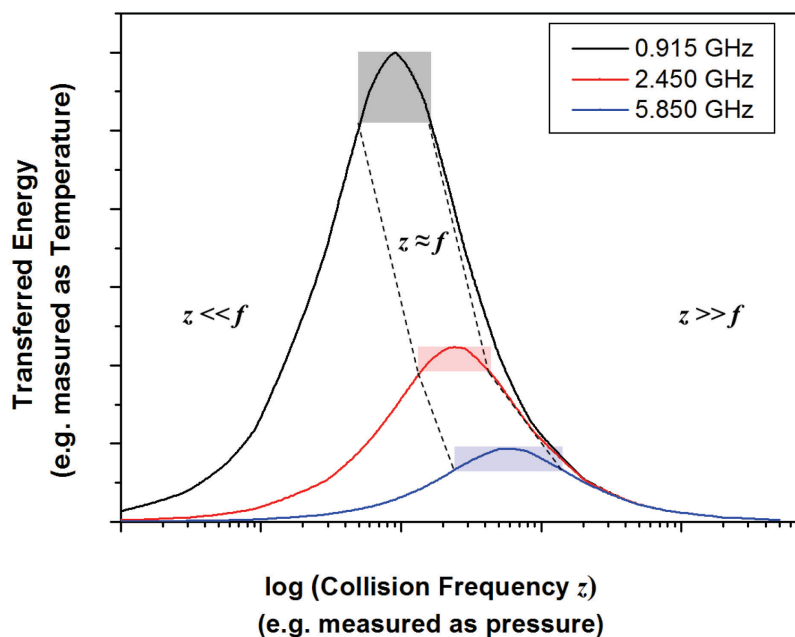
#### 4.1. Energy Transfer in a Microwave Plasma

The physico-chemical basics, elaborated for plasmas in general, can be applied to microwave plasmas in special. Therefore, the energy  $E$ , transferred to a charged species of mass  $m$  in an oscillating electrical field with frequency  $f$  is proportional to its charge  $Q$ , and inversely proportional to its mass  $m$  and the squared frequency  $f$  and is a measure of the temperature [19]. In addition to ions and free electrons, a microwave plasma consists of neutral gas species, as well as dissociated gas and finally also precursor molecules for the desired chemical reaction. Therefore, collisions between charged (electrons, ions) and uncharged species (molecules, atoms, or particles) influence the energy transfer to the particles. In this case, the collision frequency  $z$ , which is proportional to the gas pressure  $p$ , has to be considered additionally [19]:

$$E \propto \frac{Q}{m} \frac{z}{f^2 + z^2} \quad (1)$$

As the collision frequency increases with increasing gas pressure, the transferred energy is also a function of the gas pressure. Because of the significant temperature differences of the electrons and the ions, respectively neutral species, plasmas generated with microwaves are considered as non-equilibrium plasmas, or as non-thermal plasmas. They are often called “cold plasma”. These low overall temperatures in microwave plasmas are one reason for the reduced tendency of particle agglomeration during particles synthesis.

Figure 3 shows schematically the calculated relation between the collision frequency  $z$  and transferred energy  $E$  on an elementary species applying the two common industrial microwave frequencies, 0.915 GHz, and 2.45 GHz, and, additionally, the less common industrial frequency 5.85 GHz, respectively, and the three different regions of collision frequency to microwave frequency relationship. With increasing frequency the transferred energy decreases: in consequence for nanoparticle synthesis in a microwave plasma, a lower microwave frequency leads to higher reaction temperatures. Lower synthesis temperatures can be realized with higher frequencies. Generally, with increasing gas pressure (meaning collision frequency) the transferred energy increases for  $z \ll f$ , exhibits a maximum at  $f = z$ , and decreases for  $z \gg f$  [9,66,67].

**Figure 3.** Transferred energy as a function of frequency, calculated using Equation (1).

Most of the theoretical considerations on electrical charging of particles, on coagulation, or selective particle heating have been developed for non-thermal low pressure RF plasmas [47,68–71]. Analogous considerations for microwave plasmas are seldom, but exist. Vollath [67] showed in model calculations, that charging of particles in a microwave plasma depends on the collision frequency, respectively pressure. Experimental evidence for narrow particle size distribution applying microwave plasma synthesis methods was shown from several groups [48,72–76]. It is, therefore, most likely that findings for RF plasmas related to particle charging, coagulation, or selective particle heating are transferable to microwave plasmas.

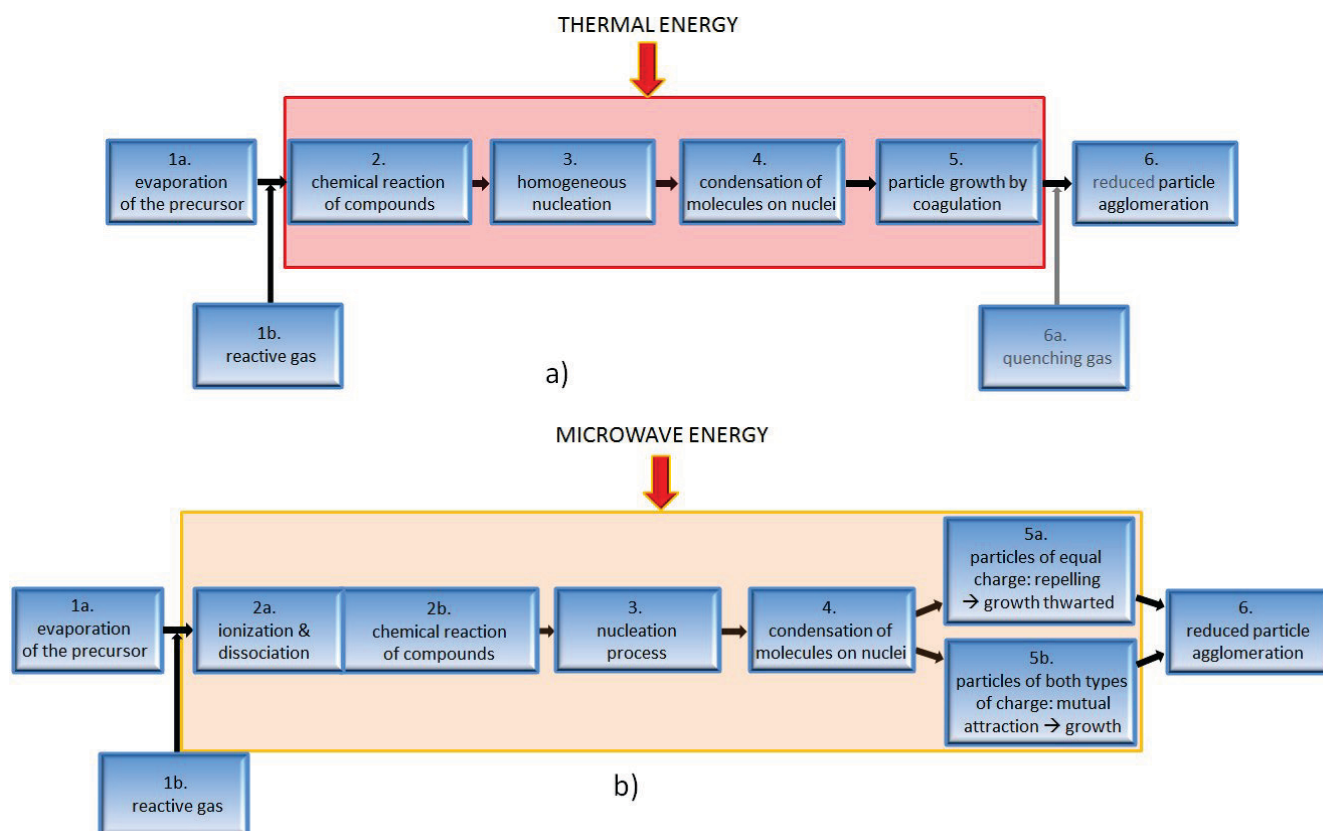
#### 4.2. Impact of Microwave Plasma on Particle Formation

As the microwave plasma process is a gas phase process, a vaporized precursor is the starting material. The microwave plasma provides a chemically highly reactive environment, because the presence of free electrons has an impact on chemical reactions. This is demonstrated in chemical kinetic models for the dissociation of silane and hydrogen in RF plasmas [69]. Particles can be synthesized rapidly due to the high degree of chemical dissociation and ionization of the compounds involved in chemical reaction. Thermodynamically possible, but kinetically thwarted reactions can occur at relatively moderate temperatures.

The single steps of a gas-phase reaction are illustrated schematically in Figure 4a. A volatile precursor is evaporated (step 1a), and an appropriate reactive gas is introduced (step 1b). Thermal energy is applied to ignite and conduct the chemical reaction of the compounds (step 2). After this step molecules collide, and particles, respectively crystallites are formed by a homogeneous nucleation process (step 3). The particles then grow by condensation of molecules on the nuclei (step 4), and further particle growth happens by coagulation (step 5), respectively coalescence. Finally,

agglomeration of particles (step 6) occurs. Particle agglomeration can be reduced, when a quenching step (step 6a) is added.

**Figure 4.** Visualization of the general steps of particle formation occurring in gas phase reactions. Thermally supported gas-phase reactions with optional quenching step (a). Microwave plasma generated gas-phase reactions (b).

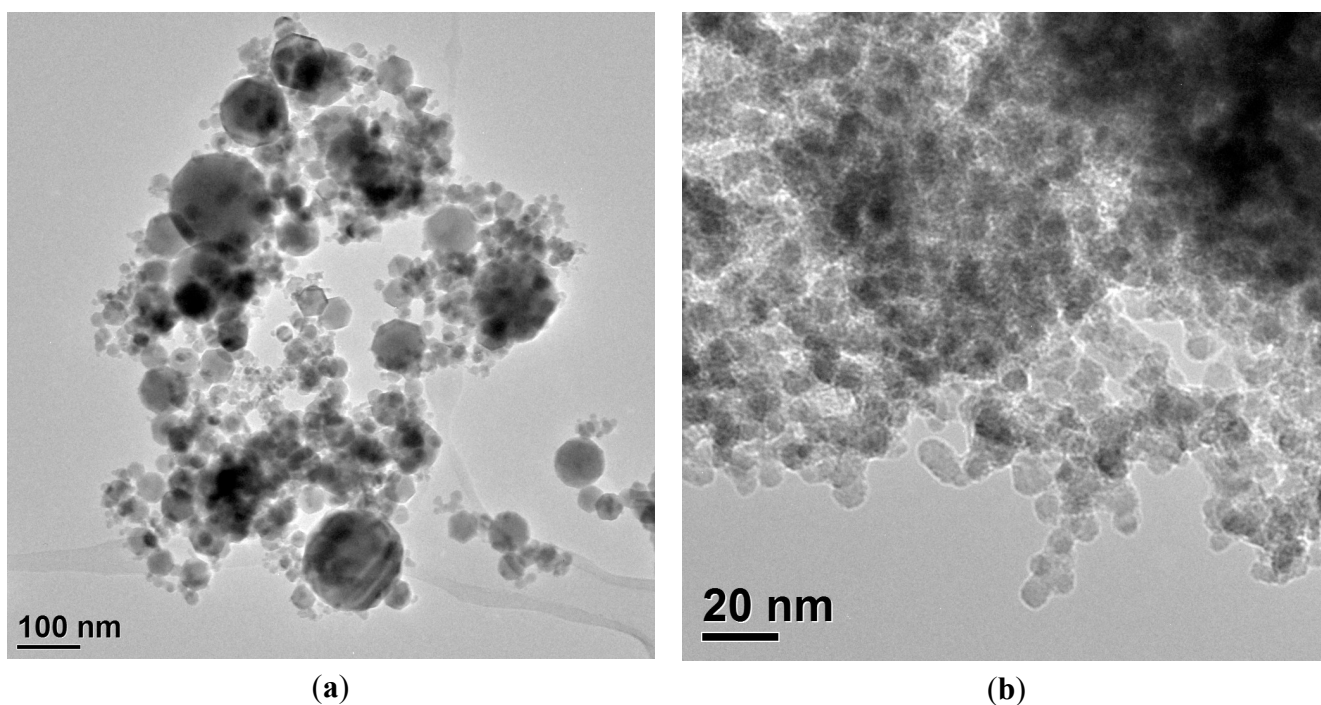


In a microwave plasma, the steps of particle formation in gas phases are supported by the ionization and dissociation of the compounds, as well as a particle charging in the plasma. This is schematically shown in Figure 4b. The critical step for particle formation is the nucleation. The variation of particle size is correlated with changes in number concentration of nuclei in the plasma. According to Kortshagen [20], the nucleation process seems to be different from situations described by classical homogeneous nucleation from super-saturated vapor. The nanoparticle formation in plasmas seems rather describable as a chemical clustering process, which is determined by reactions of chemical key species. These species will be different for each materials system. Therefore, general statements for cluster formation in plasmas seem nearly impossible. Synthesis conditions can be selected in such a way that resulting particles carry electrical charges of the same sign (see Figure 3). Then, the unipolar particle charge prevents particle growth by coagulation or coalescence and particle agglomeration [20]. Vollath's model calculation results [67] lead to the conclusion that the width of size distribution of particles produced with plasma (RF or microwave) processes is about 50% narrower compared to conventional gas phase processes, under condition that particles carry charges of equal signs. Therefore, very small particles (nanoparticles) with a narrow particle size distribution can be expected using non-thermal microwave plasmas as compared to conventional gas-phase processes and aerosol

processes. As the temperature is low, a sintering of the particles (formation of hard agglomerates) is not occurring. A typical example is shown in Figure 5, where particles synthesized in a conventional gas-phase process show larger particles and broader particle size distribution (Figure 5a) compared to nanoparticles synthesized in a low pressure microwave plasma (Figure 5b).

In addition, particle charging discussed in literature as an advantage in non-thermal plasmas [20,67,71], another advantage for nanocrystal formation in non-equilibrium plasma is discussed: the selective particle heating [70]. According to Kortshagen's explanations for non-thermal plasmas [20] energetic surface reactions, such as electron-ion recombination and surface chemical reactions, may lead to an intense heating of the particles. Nanoparticles in non-thermal plasmas can be heated to temperatures that exceed the temperature of the surrounding gas by several hundreds of kelvin. In contrast, the cooling processes through convection or conduction and radiation are relatively inefficient. Therefore, particles can crystallize in low-temperature plasmas, although the plasma temperature is below crystallization temperature. Mangolini and Kortshagen [70] show simulated evidence for the size dependence of the nanoparticle temperature of Si-nanoparticles. They conclude that selective heating of nanoparticles essentially explains the formation of crystallized nanoparticles with high crystallization temperature in a low-temperature plasma with gas temperatures lower than crystallization temperature. Experimental evidence for crystallinity is shown from different research groups for several nanomaterials that exhibit crystalline particles, such as  $ZrO_2$ ,  $SnO_2$ , or  $HfO_2$ .

**Figure 5.** Transmission electron microscopy images of (a) commercially available  $Fe_2O_3$  nanopowder made by a gas-phase process (method not specified; supplier: Sigma-Aldrich, order number 544884-25g/Lot 05223EE) and (b)  $Fe_2O_3$  nanoparticles synthesized in a low pressure 2.45 GHz microwave plasma. The difference between the two materials is evident. The average particle size of the low pressure microwave plasma made particles is significantly smaller, and their particle size distribution is much narrower compared to the commercial powder.



### 4.3. Influence of Process Parameters on the Resulting Product

The discussion of experimental parameters in microwave plasma synthesis of nanoparticles is quite complex: it comprises as well microwave frequency and cavity design (both related to the equipment design), as the system temperature, the microwave power, the system pressure, the residence time, the precursor type, and the precursor concentration in the system. Many parameters are interdependent. This means e.g., increasing the gas-flow of the reaction gas increases not only the gas-pressure, but also the temperature, influencing on its part the collision conditions, as well as residence time in the reaction zone. Furthermore, the temperature of the system can be influenced directly by the applied microwave power. These interdependences are additionally overlapped by the influence of the pressure on particle charging and selective particle heating.

#### 4.3.1. Criteria How to Choose a Precursor

The considerations for precursor selection are general and may apply for each desired nanoparticle synthesis. Most favorable are gaseous precursors, but only a few compounds, as silane ( $\text{SiH}_4$ ) for the synthesis of Si-based nanoparticles, or methane ( $\text{CH}_4$ ), acetylene ( $\text{HC}\equiv\text{CH}$ ) and ethylene ( $\text{H}_2\text{C}=\text{CH}_2$ ) for the synthesis of carbonaceous matter, are gases. Most of the relevant and commonly used precursors are liquids or solids with high vapor pressure: mainly water-free chlorides, metal-carbonyls, and different organometallic precursors. The liquids can be fed accurately via syringe pumps. In principle, precursors used in CVD synthesis [77–79] are to some extent suitable as precursors for microwave plasma reactions. Table 1 shows a variety of solid, liquid and gaseous precursors with some relevant data. All precursors must be handled under careful conditions with personnel protection measure, as all are either toxic or very toxic, or at least irritant or harmful for human health, and also partly sensitive to atmosphere. Thus, toxicity is certainly one aspect one has to consider for precursor selection.

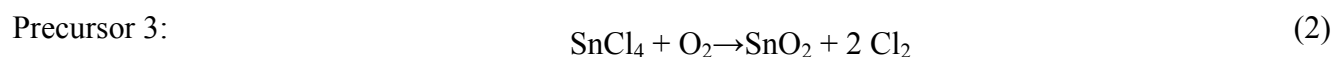
**Table 1.** Selection of different commercially available, solid, liquid, or gaseous, and volatile precursors typically used in microwave plasma nanoparticle synthesis.

No.	Chemical formula [CAS-Number]	Name/synonym	Melting point/boiling point	Aggregate state	Remarks and hazards
1	$\text{FeCl}_3$ [7705-08-0]	Iron(III)chloride	304 °C/319 °C 120 °C sublimation	solid	Corrosive; hygroscopic; harmful; releases Cl
2	$\text{SiCl}_4$ [10026-04-7]	Silicon(IV)chloride Silicon-tetrachloride	−70 °C/57 °C	liquid	Moisture sensitive; corrosive to metals and tissues; irritant; releases Cl Moisture and air sensitive;
3	$\text{SnCl}_4$ [7646-78-8]	Tin(IV)chloride Tin-tetrachloride	−33 °C/114 °C	liquid	corrosive to metals and tissues; harmful; irritant; releases Cl

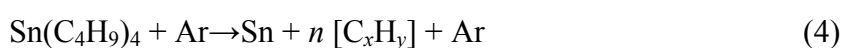
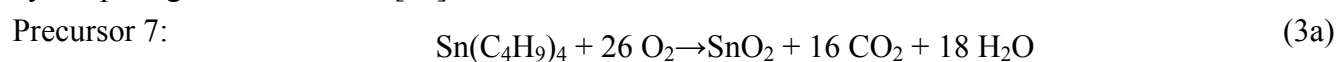
Table 1. Cont.

No.	Chemical formula [CAS-Number]	Name/synonym	Melting point/boiling point	Aggregate state	Remarks and hazards
4	TiCl <sub>4</sub> [7550-45-0]	Titanium(IV) chloride Titanium-tetrachloride	−25 °C/136 °C	liquid	Moisture sensitive; corrosive to metals and tissues; irritant; releases Cl
5	Fe(CO) <sub>5</sub> [13463-40-6]	Ironpentacarbonyl	−20 °C/103 °C	liquid	Air sensitive; highly flammable; very toxic
6	SiH <sub>4</sub> [7803-62-5]	Mono-Silane Silicon-tetrahydride	−187 °C/−112 °C	gaseous	Extremely flammable; pyrophoric in air
7	Sn(C <sub>4</sub> H <sub>9</sub> ) <sub>4</sub> [1461-25-2]	Tetra- <i>n</i> -butyltin	−97 °C/145 °C @ 10 mm Hg pressure	liquid	Harmful; toxic
8	Ti(OC <sub>4</sub> H <sub>9</sub> ) <sub>4</sub> [5593-70-4]	Titanium(IV)- <i>n</i> - butoxide	−55 °C/206 °C @ 10 mm Hg pressure	liquid	Moisture sensitive; flammable; irritant
9	Zr(OC <sub>4</sub> H <sub>9</sub> ) <sub>4</sub> [2081-12-1]	Zirconium(IV)- <i>t</i> - butoxide	3 °C/90 °C @ 5 mm Hg pressure	liquid	Moisture sensitive; irritant
10	HC≡CH [74-86-2]	Acetylene	−82 °C (sublimation)	gaseous	Flammable; may cause fire flash
11	CH <sub>4</sub> [78-82-8]	Methane	−182 °C/−164 °C	gaseous	Flammable; explosive
12	H <sub>2</sub> C=CH <sub>2</sub> [78-85-1]	Ethylene	−169 °C/−103 °C	gaseous	Highly flammable; may form explosive mixtures with air

Another selection criterion is, besides the boiling point, the theoretical conversion of product per unity of precursor and the resulting by-products. Therefore, one has to look at the chemical reactions which may occur in the plasma during a complete or incomplete reaction. This is shown exemplarily for the reaction of SnCl<sub>4</sub>, respectively Sn(C<sub>4</sub>H<sub>9</sub>)<sub>4</sub>. Taking into account the densities of SnCl<sub>4</sub> (2230 kg/m<sup>3</sup>) and Sn(C<sub>4</sub>H<sub>9</sub>)<sub>4</sub> (1050 kg/m<sup>3</sup>), e.g., the oxide yield of 1 mL precursor is 2.4 times higher for SnCl<sub>4</sub> than for Sn(C<sub>4</sub>H<sub>9</sub>)<sub>4</sub>. Identical precursor concentrations therefore do not mean identical reactive Sn-cation concentration. Thus, an influence on particle size is expected, depending on the precursor used. In addition, the by-products have to be taken into account. This is explained exemplarily by means of two different Sn-precursors:



Using SnCl<sub>4</sub> as precursor, chlorine is the residual by-product (Equation 2), which can be removed by tempering in air at 300 °C [54].



Using  $\text{Sn}(\text{C}_4\text{H}_9)_4$  as precursor, the scope is wide. A complete reaction, meaning synthesis conditions where the whole precursor is oxidized, yields into  $\text{CO}_2$  and  $\text{H}_2\text{O}$  as by-products (Equation 3a). Synthesis conditions can be selected to yield in incompletely decomposed  $\text{Sn}(\text{C}_4\text{H}_9)_4$  precursor in form of residual hydrocarbons (Equation 3b) Finally, metallic Sn particles with hydrocarbons as by-product can be synthesized using pure Ar as plasma gas (Equation 4). The real suitability of a precursor for particle synthesis finally is also affected by capability of nuclei formation under the selected experimental conditions. Therefore, experiments to test the ability of a precursor are always necessary, and have to be considered also in the context of materials application.

#### 4.3.2. Influence of Precursor Concentration

Changing the precursor concentration mainly means changing collision frequency between atoms, reactive molecules, ions, and electrons in the plasma. Therefore, a strong impact of this parameter on the number concentration, respectively nuclei formation, and the particle size is expected. For different synthesized materials, several research groups find comparable behavior for the dependency of nanoparticle sizes from the precursor concentration using different 2.45 GHz equipment. Mostly investigated are the particle sizes of  $\text{Fe}_2\text{O}_3$  [72,80], Si [49,81],  $\text{SiO}_2$  [80], GaN [82] and  $\text{SnO}_2$  [83] nanoparticles as a function of precursor concentration. In all cases, the observed particle, respectively the crystallite sizes, do not exceed 12 nm (p. 288 in [21]). As a rule of thumb triplicate the precursor concentration doubles the particle volume [72,80] for  $\text{Fe}_2\text{O}_3$  made from  $\text{Fe}(\text{CO})_5$ . The tendency of increased particle size with increasing precursor concentration is also confirmed by theoretical considerations for the formation of SiC in an atmospheric pressure plasma [84]: a strong positive impact of precursor concentration on particle size is calculated. This is also modeled in low-pressure plasma for Si-particles [49].

For the dependency of particle size from precursor concentration general rules can be stated, independent from the material synthesized, independent from the research groups, and even independent from the pressure in the microwave plasma: with increasing precursor concentration an increase in particle size is observed. At a very low concentration particle sizes around 2 nm can be realized, whereas an increase of several orders of magnitude in precursor concentration is necessary to produce particles with sizes around 5–10 nm.

#### 4.3.3. Influence of Microwave Power, Pressure, Temperature, and Residence Time

The influence of microwave frequency with respect to the temperature is given by Equation (1). This means a generally lower reaction temperature and shorter residence time for a synthesis performed at 2.45 GHz compared to one performed at 0.915 GHz. As the syntheses usually are operated at one fixed frequency and a constant experimental set-up, these factors are not further discussed.

Experimental evidence for decreasing particle size with increasing microwave power is given for several materials investigated from different groups. Janzen *et al.* [72] and Thekedar [80] show this behavior for  $\text{Fe}_2\text{O}_3$  nanoparticles, Kleinwechter *et al.* [73] for ZnO nanoparticles, Knipping *et al.* [81] for Si nanoparticles, Thekedar [80] for  $\text{SiO}_2$  nanoparticles, and Shimada *et al.* [82] for GaN nanoparticles. In all cases measured particle sizes are below 10 nm. Although in all cases the size difference seems marginal, the reduction in particle volume is significant. Doubling the microwave

power reduces the particle volume by a factor of approximately 2 for  $\text{Fe}_2\text{O}_3$  [72] and for ZnO [73]. Decreasing particle sizes with increasing microwave power in addition, is supported by theoretical calculations in an atmospheric microwave plasma for SiC formation [84] and in low pressure plasma for Si formation [49]. The reason for the pronounced influence of microwave power on particle size might be a slow chemical reactivity at low microwave power, resulting in a smaller number of nuclei [82]. The molecules which are formed by the chemical reaction condense on the few nuclei, leading to larger particles. In the case of higher microwave power a faster chemical reaction rate leads to more nuclei, resulting in a larger amount of smaller particles.

In addition to its influence on particle size, microwave power also affects the degree of chemical conversion, especially when using organometallic precursors with high organic fraction. This was observed for the synthesis of  $\text{SnO}_2$  made from  $\text{Sn}(\text{C}_4\text{H}_9)_4$  under several experimental conditions [60]. A higher microwave power yielded in whiter powder, containing less unreacted organic residuals at the surface of the particles whereas lower microwave power resulted in gray powder. Analysis by different analytical methods revealed residual hydrocarbons on the surface of the nanoparticles [60].

With increasing pressure a linear increase of the diameter of the nanoparticles is observed for Si [81], ZnO [73],  $\text{SiO}_2$  [80], and  $\text{Al}_2\text{O}_3$  [85] nanoparticles from several groups. This behavior can be explained by the increased collision probability, leading to enhanced nanoparticle growth.

The variation of residence time due to experimental parameters as microwave power, pressure, or temperature is only marginal. Therefore, a strong influence of residence time on particle size cannot be expected. A significant increase of residence time can only be realized by either increasing the length of the reaction zone, or by using two or more plasma zones consecutively, as shown by Schlabach *et al.* [86].

#### 4.4. Microwave Components and Experimental Set-Up

Experimental set-ups for the synthesis of nanoparticles can be realized with standard industrial frequencies of 0.915 (wavelength  $\lambda \sim 32$  cm), and 2.45 GHz ( $\lambda \sim 12$  cm, household kitchen frequency). Microwave generators, magnetrons, appropriate wave guides, and passive components such as isolators, directional couplers, tri-stub tuners, or sliding shorts are components which are commercially available worldwide from several suppliers. For a simple set-up, a magnetron with an appropriate power supply, an isolator, a directional coupler, a tri-stub tuner and an appropriate resonant cavity are needed. Resonant cavities (applicators) are also commercially available to some extent. Examples for commercially available cavities are downstream sources, plasma torches, surfatrons, or surfaguides. In many cases, cavities are a special and individual custom design, depending on the needs of the customer.  $\text{TE}_{01}$  mode cavities can be adjusted to the maximum of the E-field vector at the centerline of the reaction tube using a sliding short and a tri-stub tuner [87]. Using a specially developed  $\text{TE}_{11}$  rotating mode cavity [88], a tuning with sliding short is not necessary anymore.

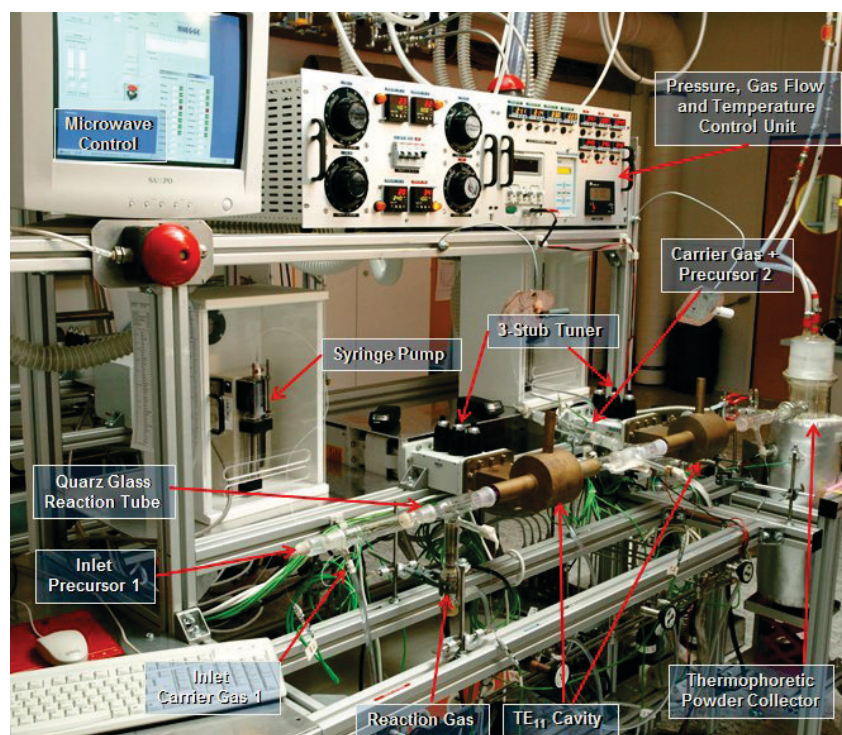
The plasma zone itself is made of quartz glass, or alternatively another suitable dielectric material, having low losses at microwave frequencies. The advantage of glass is its transparency, permitting the observation of reactions in the plasma. The plasma zone passes the cavity and at the intersection the plasma is ignited.

In consequence, the selected microwave frequency of the equipment, the type of cavity, and the length of the reaction zone are defined by the equipment in use. The chosen precursor, the used gas

pressure, the precursor concentration, and the energy input (microwave power) are the main tools for proper setting of experimental conditions to achieve optimum synthesis conditions for each material. To produce small nanoparticles with narrow size distribution, pressure conditions should be selected in the range of equal charges, so that particles can repel each other to thwart particle growth.

Figure 6 shows, exemplarily, a  $2 \times 2$  kW 2.45 GHz experimental equipment for the synthesis of ceramic core/ceramic shell nanoparticles. Further details for this set-up and other set-up modifications (e.g., for the synthesis of ceramic core/organic shell nanoparticles) are described by Szabó [21].

**Figure 6.** Experimental 2.45 GHz set-up using 2 consecutive  $TE_{11}$  cavities for the synthesis of core/shell nanoparticles and thermophoretic powder collection, as it is used in Karlsruhe.



The bottle-neck in the synthesis of nanoparticles in microwave plasma is the particle collection. Aerosol methods of powder collection, as the collection via thermophoresis [10,89] are quite common. Thermophoresis can be considered as a removing of small particles from a gas stream [90,91]. The particles are transported in a temperature gradient. The effect is as more efficient as the temperature gradient is. Other factors of influence are the thermal conductivity, the diameter, the mass of the particles, and the gas flow rate, respectively. The larger the particle diameters are, and the higher their mass is, the better they can be collected via thermophoresis. Mechanical filtering [81,92] or cyclones [93,94] are alternative collection methods for nanoscaled powders. A common method for deposition of small charged particles from the gas phase is electrostatic deposition [95,96]. Further applied collection methods are the direct dispersion of nanoparticles in appropriate liquids (e.g., resins, glycols, liquid polymers) [97,98], and the deposition of nanoparticles on substrates, forming porous nanoparticle layers without liquid processing [54,99,100].

Only few remarks are found in literature concerning commercialization of microwave plasma synthesis method and the potential for up-scaling. The “Microwave Plasma Synthesis Machine”

(NANOGEN<sup>®</sup> approach, (<http://www.matmod.com/index.html>, last access 6 June 2014) is characterized by a production rate of 50 g/h for Fe-nanoparticles [101]. David *et al.* [102] reported a yield of 1 g  $\gamma$ -Fe<sub>2</sub>O<sub>3</sub> with microwave plasma synthesis at low pressure for one experiment. Using an atmospheric microwave plasma torch a yield of 1 g/h  $\epsilon$ -Fe<sub>2</sub>O<sub>3</sub> is reported [103]. Reaction rates between 50 and 100 g/h for 915 MHz equipment are reported by Vollath and Szabó (page 237 in [89]) for particles with sizes above 5 nm. Petermann *et al.* [59] apply a commercially available plasma source and reach 0.7 to 10 g/h powder output. A similar order of magnitude concerning the output is also mentioned by Bywalez *et al.* [104].

## 5. Materials Synthesized in Microwave Plasma

### 5.1. Tabular Overview on Literature Data

In this section a publication overview will be given on materials synthesized using microwave plasma (Tables 2–6). Most papers are found on the synthesis of oxide nanoparticles, followed by nitrides, and metallic nanoparticles. The tables are complemented by other gas-phase plasma methods, to give a better overview.

**Table 2.** Overview on published papers related to the subject of oxide nanoparticles, synthesized in microwave plasmas.

Oxides	MW low pressure plasma		MW atmospheric pressure	RF plasma	DC thermal plasma
	2.45 GHz	0.915 GHz			
Fe <sub>2</sub> O <sub>3</sub>	[40,72,102,105,106]	[107,108]	[52,102,103,109–111]	[112]	[113–115]
ZrO <sub>2</sub>	[74,116–120]	[41,42]			
Al <sub>2</sub> O <sub>3</sub>	[42,43,85,118]	[41]		[121]	
SnO <sub>2</sub>	[54,60,83,122]				[123]
TiO <sub>2</sub>	[120,124]	[41]	[55,56,125,126]	[127]	
ZnO	[48,73,128]		[129,130]	[131,132]	
Cr <sub>2</sub> O <sub>3</sub>		[133]			
TeO <sub>2</sub>			[134]		
MgO			[135]		
V <sub>2</sub> O <sub>5</sub>			[130,136]		
WO <sub>3</sub>	[137]				[138]
GeO <sub>2</sub>	[48]				
HfO <sub>2</sub>	[119]				

**Table 3.** Overview on published papers related to the subject of non-oxide nanoparticles, synthesized in microwave plasmas.

Materials	MW low pressure plasma		MW atmospheric pressure	MW not specified	RF plasma	DC thermal plasma
	2.45 GHz	0.915 GHz				
<i>Nitrides</i>						
GaN	[139]		[82,140]			
TiN			[141–143]	[144]	[145]	
ZrN		[146]		[144]		
BN	[147]					
VN			[142,148]			
Si <sub>3</sub> N <sub>4</sub>			[142]		[149]	
AlN						[150,151]
other			[152]			
<i>Carbides</i>						
SiC	[86,153]		[84]		[154–157]	[156,158–161]
B <sub>4</sub> C					[162]	
Fe-carbides					[163]	
<i>Carbon Materials</i>						
amorphous C	[164,165]					
carbonaceous					[166]	
graphite	[165]			[167]		
graphene			[63]			
diamond	[33,35,165]			[168]		
fullerenes	[169]					

**Table 4.** Overview on published papers related to the subject of chalcogenide nanoparticles, synthesized in microwave plasmas.

Chalcogenides	MW low pressure plasma	
	2.45 GHz	0.915 GHz
MoS <sub>2</sub>	[170]	[170]
WS <sub>2</sub>	[170–172]	[170,171]
ZrS <sub>2</sub>	[172]	
HfS <sub>2</sub>	[172]	
ZrSe <sub>2</sub>	[171]	
SnS <sub>2</sub>	[171]	
MoSe <sub>2</sub>	[171]	
WSe <sub>2</sub>	[171]	[171]

**Table 5.** Overview on published papers related to the subject of metal nanoparticles, synthesized in microwave plasmas.

Metals	Low pressure plasma 2.45 GHz	MW atmospheric pressure	MW not specified	RF plasma	DC thermal plasma
Fe	[40,45,101,173]	[174]	[175]	[95,176]	[95]
Al		[177]			
Si	[49,59,81,104]	[143]		[178–182]	
Ge				[183–185]	
In	[186]				
Zn					
Cu		[187]			
Mo		[187]			
W		[187]			
Ag			[188]		[189]
Co	[45]		[175,190]		
Ni			[191]		
bimetallic particles	[45]	[187]	[175,191]	[192,193]	

**Table 6.** Overview on published papers related to the subject of composite nanoparticles, synthesized in microwave plasmas.

Composite materials	MW low pressure plasma		MW atmospheric pressure	MW not specified	RF plasma	DC thermal plasma
	2.45 GHz	0.915 GHz				
Coated or Core/Shell Nanoparticles	[51,81,97,194–202]	[44,117,203]	[63,204]	[190]	[205]	
Binary Oxides				[206]		
Doped Particles	[57,116,207]		[208]		[209–212]	[213]
Complex/Composite Particles	[214]		[63,111,215]			[216]

## 5.2. Materials and Properties

As many physical properties of materials are size dependent, particle size, respectively, particle size distribution is a very important factor in the synthesis of nanoparticles. The most striking difference between commercially available gas-phase synthesized nanoparticles and those nanoparticles, made in a microwave plasma in a low pressure system is the particle size distribution (compare Figure 5). Commercial powders usually contain nanoparticles of sizes ranging from around 5 nm to approximately 200 nm. Similar, broad particle size distributions are observed, when using microwave torches [52,103,109,110], whereas the powders synthesized in low pressure microwave plasma are often characterized by a very narrow particle size distribution [105,107,108,198]. This can be observed for several commercially available nanoscaled powders, like Fe<sub>2</sub>O<sub>3</sub>, ZrO<sub>2</sub>, SnO<sub>2</sub>, or TiO<sub>2</sub>. In consequence, the size dependent properties are selective adjustable in microwave plasma synthesized particles. In the following section, several examples will explain why and how proper selection of

experimental parameters is necessary to influence nanoparticle properties, especially with respect to application relevant properties. The first example will be from the area of magnetic nanoparticles, the second example will show results on luminescence properties of core/shell nanoparticles, and the last example will present results on the development of nanoparticles as anode materials.

### 5.2.1. Superparamagnetic Iron Oxide Nanoparticles

Superparamagnetism is a property of single, isolated, small magnetic particles [217]. It is caused by thermal fluctuations of the magnetization vector in a zero field, when the thermal energy of the particle is larger than the energy of magnetic anisotropy [218]. Therefore, magnetization curves show only diminishing magnetic hysteresis. The magnetic properties of ferrite nanoparticles are known to be size dependent [219–222]. Their saturation magnetization usually is below the saturation magnetization of the bulk counterpart material. With decreasing particle size, respectively particle volume, the saturation magnetization decreases drastically. This is because the ferrite nanoparticles are covered by a nonmagnetic surface layer of around 0.5 to 1 nm thickness [223,224]. With decreasing particle size the amount of nonmagnetic specific surface area increases. This is leading to the reduction of saturation magnetization.

Iron oxide nanoparticles are those particles, whose synthesis and properties are described from several research groups using the whole band width of plasma types (see also Table 2). This material has potential for application in catalysis [225], and due to its magnetic properties in biomedical applications [226]. Papers dealing with microwave gas phase syntheses or plasma syntheses of magnetic nanoparticles show a heterogeneous field of results, ranging from “large” nanoparticles with saturation magnetization near the bulk saturation magnetization, to “small” nanoparticles with saturation magnetization far away from the bulk value. The found data on magnetization and particle sizes fit quite well in the general trends of size dependent magnetic properties (Figure 7). Those particles made from a chloride precursor [107,108] deviate from the trend. According to the indicated particle sizes, the saturation magnetization should be higher. The extreme low saturation magnetization is explained with a lattice disorder in the occupation of tetrahedral and octahedral lattice sites by  $\text{Fe}^{3+}$  ions. In this case, obviously, the chloride precursor is not suited for the synthesis of a good material. The literature results are summarized in Table 7.

**Table 7.** Fe<sub>2</sub>O<sub>3</sub> nanoparticles and the relevant properties particle size and magnetization.

Author	Material and precursor	Plasma type	Particle size	Magnetic properties
Li <i>et al.</i> [52]	$\gamma$ -Fe <sub>2</sub> O <sub>3</sub> from Fe(CO) <sub>5</sub>	2.45 GHz, atmospheric pressure plasma jet, 1 kW	900 K: $\varnothing$ 45 nm spread 20–100 nm 1100 K: $\varnothing$ 26 nm spread 15–40 nm	not given
David <i>et al.</i> [102,109]	$\gamma$ -Fe <sub>2</sub> O <sub>3</sub> from Fe(CO) <sub>5</sub>	2.45 GHz, atmospheric pressure torch 140 W	30–100 nm	293 K(1 T) $\sigma_s = 66.6$ Am <sup>2</sup> /kg 4 K(1 T): $\sigma_s = 77.0$ Am <sup>2</sup> /kg
Synek <i>et al.</i> [110]	$\gamma$ -Fe <sub>2</sub> O <sub>3</sub> from Fe(CO) <sub>5</sub>	2.45 GHz, atmospheric pressure torch 180 W	$\varnothing$ 12 nm spread 5.5–20 nm	not given
David <i>et al.</i> [103]	$\epsilon$ -Fe <sub>2</sub> O <sub>3</sub> from Fe(CO) <sub>5</sub>	2.45 GHz, atmospheric pressure torch 230 W	10–100 nm	not given
Synek <i>et al.</i> [111]	Fe <sub>3</sub> O <sub>4</sub> and/or $\gamma$ -Fe <sub>2</sub> O <sub>3</sub> from Fe(CO) <sub>5</sub>	2.45 GHz, atmospheric pressure torch 310 W	5–21 nm	not given
Chou & Phillips [40]	Fe <sub>2</sub> O <sub>3</sub> from Ferrocene	2.45 GHz low pressure plasma 3000 Pa, 200 W	10–100 nm	not given
Janzen <i>et al.</i> [72]	$\gamma$ -Fe <sub>2</sub> O <sub>3</sub> from Fe(CO) <sub>5</sub>	2.45 GHz low pressure plasma 3000 Pa	80 W: 5.3 nm 160 W: 4.1 nm	not given
David <i>et al.</i> [102]	$\gamma$ -Fe <sub>2</sub> O <sub>3</sub> from Fe(CO) <sub>5</sub>	2.45 GHz low pressure plasma 4000 Pa, 650 W	20–80 nm	293 K(1 T) $\sigma_s = 59.9$ Am <sup>2</sup> /kg 4 K(1 T) $\sigma_s = 69.3$ Am <sup>2</sup> /kg
Nadeem <i>et al.</i> [105]	$\gamma$ -Fe <sub>2</sub> O <sub>3</sub> from Fe(CO) <sub>5</sub>	2.45 GHz low pressure plasma	$\varnothing$ 6 nm spread 3–10 nm	300 K(5 T) $\sigma_s = 42$ Am <sup>2</sup> /kg 4.2 K(5 T) $\sigma_s = 51$ Am <sup>2</sup> /kg
Vollath <i>et al.</i> [107]	$\gamma$ -Fe <sub>2</sub> O <sub>3</sub> from FeCl <sub>3</sub>	0.915 GHz low pressure plasma	4–5 nm	300 K(1 T) $\sigma_s = 2.7$ Am <sup>2</sup> /kg 10 K(1 T) $\sigma_s = 4.3$ Am <sup>2</sup> /kg
Vollath <i>et al.</i> [108]	$\gamma$ -Fe <sub>2</sub> O <sub>3</sub> from FeCl <sub>3</sub>	0.915 GHz low pressure plasma 3000 Pa	6–8 nm	300 K(1 T) $\sigma_s = 3.4$ Am <sup>2</sup> /kg 10 K(1 T) $\sigma_s = 6.4$ Am <sup>2</sup> /kg
Vollath <i>et al.</i> [108]	$\gamma$ -Fe <sub>2</sub> O <sub>3</sub> from Fe <sub>3</sub> (CO) <sub>12</sub>	0.915 GHz low pressure plasma 3000 Pa	4–6 nm	300 K(1 T) $\sigma_s = 16.0$ Am <sup>2</sup> /kg 10 K(1 T) $\sigma_s = 18.9$ Am <sup>2</sup> /kg
Banerjee <i>et al.</i> [114]	$\gamma$ -Fe <sub>2</sub> O <sub>3</sub> from Fe-metal	DC thermal plasma	10–100 nm	300 K(1.5 T) $\sigma_s = 79$ Am <sup>2</sup> /kg
Lei <i>et al.</i> [115]	Fe <sub>3</sub> O <sub>4</sub> and/or $\gamma$ -Fe <sub>2</sub> O <sub>3</sub> from Ferrocene	DC thermal plasma torch	8–9 nm	293 K(1.5 T) $\sigma_s = 40$ Am <sup>2</sup> /kg 10 K(1.5 T) $\sigma_s = 43$ Am <sup>2</sup> /kg

**Figure 7.** Room temperature saturation magnetization as a function of particle size. Reference data for particle size dependent saturation magnetization (all symbols in black color) are taken from Han *et al.* [220], Morales *et al.* [222], and de Montferrand *et al.* [227], and finally the bulk reference value is taken from [228], page 993. Literature data of the diverse plasma synthesized  $F_2O_3$  nanoparticles (colored symbols) are taken from Table 7 (David *et al.* [102,109], Nadeem *et al.* [105], Vollath *et al.* [107,108], Banerjee *et al.* [114], Lei *et al.* [115]). The bars herein are not error bars; they show the spread of indicated particle sizes.

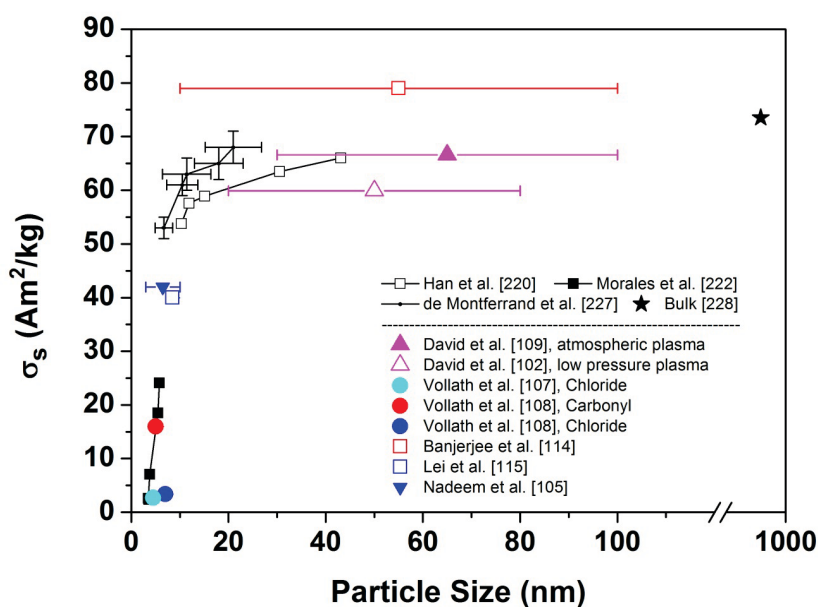


**Figure 8.** Luminescence properties (excitation wavelength 325 nm) of core/shell nanoparticles with ceramic cores made from various precursors. (a) HfO<sub>2</sub>-core/organic shell nanoparticles with different shells (b) Al<sub>2</sub>O<sub>3</sub>/anthracene/PMMA nanoparticles.

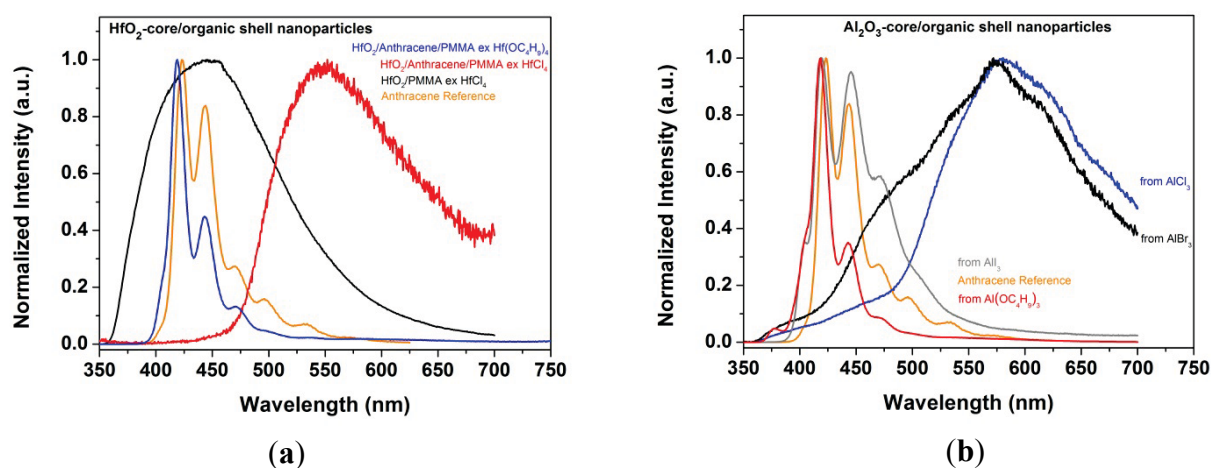


**Table 8.** Luminescence properties of various core/shell nanoparticles made from halides or organometallic precursors [199].

Core/Shell	Precursor	Spectrum type	Peak positions (nm)
Al <sub>2</sub> O <sub>3</sub> /PMMA	AlCl <sub>3</sub>	Excimer	418.5 (very broad)
ZrO <sub>2</sub> /PMMA	ZrCl <sub>4</sub>	Excimer	445 (very broad)
ZrO <sub>2</sub> /PMMA	Zr(OC <sub>4</sub> H <sub>9</sub> ) <sub>4</sub>	Excimer	408.5 (broad)
HfO <sub>2</sub> /PMMA	HfCl <sub>4</sub>	Excimer	445 (very broad)
Anthracene (reference)		Molecule	423 (M); 444; 470; 496; 533
Al <sub>2</sub> O <sub>3</sub> /Anthracene/PMMA	AlCl <sub>3</sub>	Excimer	580.5 (very broad)
ZrO <sub>2</sub> /Anthracene/PMMA	ZrCl <sub>4</sub>	Excimer	552 (very broad)
HfO <sub>2</sub> /Anthracene/PMMA	HfCl <sub>4</sub>	Excimer	546 (very broad)
Al <sub>2</sub> O <sub>3</sub> /Anthracene/PMMA	AlBr <sub>3</sub>	Excimer	576 (very broad)
Al <sub>2</sub> O <sub>3</sub> /Anthracene/PMMA	AlI <sub>3</sub>	Molecule	404 (S); 419 (M); 445.5; 470.5;
Al <sub>2</sub> O <sub>3</sub> /Anthracene/PMMA	Al(OC <sub>4</sub> H <sub>9</sub> ) <sub>3</sub>	Molecule	377; 405 (S); 418.5 (M); 443; 471
ZrO <sub>2</sub> /Anthracene/PMMA	Zr(OC <sub>4</sub> H <sub>9</sub> ) <sub>4</sub>	Molecule	405 (S); 418.5 (M); 443; 471.5
HfO <sub>2</sub> /Anthracene/PMMA	Hf(OC <sub>4</sub> H <sub>9</sub> ) <sub>4</sub>	Molecule	405 (S); 419 (M); 443; 471

(S) denotes a shoulder, and (M) denotes the maximum.

Luminescence of PMMA coated particles is characterized by a broad excimer peak. It is generated in the interface of ceramic-polymer by the carbonyl of the  $-(C=O)-O-$  bonding of the polymer to the oxide nanoparticle [197]. The luminescence maxima are positioned at significant different wavelengths than the maxima of anthracene-coated nanoparticles made from chloride or bromide precursor. Particles synthesized from iodide or butoxide precursor exhibit modified anthracene molecule spectra. The molecule spectra of aromatic ring molecules are generated by delocalized electrons in  $\pi$ -conjugated molecules. Iodine, although being a halide, obviously does not quench anthracene fluorescence.

Halide-free core/shell nanoparticles exhibit luminescence spectra resembling to that of anthracene with some significant differences concerning the intensity ratio and the position of maxima. They resemble molecule spectra of anthracene, exhibiting a slight shoulder around 405 nm, a peak maximum

appearing at 418–419 nm, and further peaks at 443 to 445 nm, and 471 nm. The most remarkable difference to the pure anthracene spectrum is the difference in the intensity ratios of the peaks. In contrast, core/shell nanoparticles made from chlorides even with different oxide cores show excimer-like spectra with broad maxima around 545 to 550 nm. It is well known that elements of the halogen group, especially chlorine, may be quenchers of fluorescence for anthracene (page 238 in [229]).

Furthermore, luminescence spectra can be influenced by the degree of organic coating. This was shown by Vollath and Szabó for pyrene as dye [198]. The spectra are changing from excitonic spectra to molecule spectra with decreasing dye coverage. For pyrene this is explained with the ability of some fluorophores to form complexes with themselves (page 9 in [229]). The suitable combination of core precursor, type and amount of organic dye molecules and additional polymer protecting coating does allow a specified particle design with tailored luminescence properties.

Bifunctional nanoparticles finally can be synthesized in microwave plasma by the combination of a magnetic core (e.g.,  $\text{Fe}_2\text{O}_3$ ), a luminescent coating (dyes as e.g., anthracene, pyrene, perylene, coumarine), and an additional protecting polymer layer. The luminescence spectrum of  $\text{Fe}_2\text{O}_3$ /Pyrene/PMMA nanoparticles suspended in  $\text{H}_2\text{O}$  is characterized by the molecule spectrum of pyrene. The magnetic properties are typical for isolated nanoparticles: they exhibit superparamagnetism. A hysteresis is not observed. Similar observations with respect of combined properties have been shown by Vollath and Szabó [74], and by Vollath [202] for anthracene-containing  $\text{Fe}_2\text{O}_3$  particles.

### 5.2.3. Sn-Based Nanocomposites for Li-Ion Battery Application

The growing demand of high capacity Li-ion batteries for automotive or stationary energy applications creates a need for new and improved electrode materials. Nanomaterials based on tin possess a very promising potential as anode material in Li-ion batteries because they exhibit in principle much higher theoretical specific capacities (e.g.,  $\text{SnO}_2$  ca.  $780 \text{ mA h g}^{-1}$  [240], Sn ca.  $994 \text{ mA h g}^{-1}$  [241]) than currently used carbon anodes ( $372 \text{ mA h g}^{-1}$  [241]). Bulk  $\text{SnO}_2$  anode material, however, shows very poor long-term cycle stability due to internal stress caused by the large volume change ( $>200\%$ ) during the alloying process from Li and Sn to  $\text{Li}_{4.4}\text{Sn}$  resulting in cracks and loss of active material. Similar observations are made for Sn bulk material. Nanoporous materials could resolve this issue because they feature local free space to compensate this volume change. One possibility to address this issue is the use of nanocomposites consisting of core/shell nanoparticles with an active core, e.g., Sn or  $\text{SnO}_2$ , and a stabilizing shell, e.g., carbon, which acts as a scaffold between the core particles. The conducting phase is added without slurry process *in situ* during the particle synthesis process. This concept was proven to work, using microwave plasma particles deposited directly on substrates [60,100,122,214,242,243].

**Table 9.** Evolution of Li-ion battery performance through targeted synthesis of nanocomposites using microwave plasma synthesis.

Material/precursor/gas	Specific capacity [ $\text{mA h g}^{-1}$ ]			References/comments
	2nd cycle	After 50 cycles	After 100 cycles (% of 2nd cycle)	
SnO <sub>2</sub> /C core/shell SnCl <sub>4</sub> /C <sub>10</sub> H <sub>12</sub> Ar/20%O <sub>2</sub>	706	238	173 (24.5%)	[100]; no drying step before battery assembly
SnO <sub>2</sub> (C <sub>x</sub> H <sub>y</sub> ) composite Sn(C <sub>4</sub> H <sub>9</sub> ) <sub>4</sub> Ar/20%O <sub>2</sub>	1186	468	404 (34.1%)	[244]; improved battery assembly
SnO <sub>2</sub> (C <sub>x</sub> H <sub>y</sub> ) composite Sn(C <sub>4</sub> H <sub>9</sub> ) <sub>4</sub> Ar/20%O <sub>2</sub>	1137	640	558 (49.1%)	[244]; vinylene carbonate (VC) addition into electrolyte
Sn(O)-C <sub>x</sub> H <sub>y</sub> Sn(C <sub>4</sub> H <sub>9</sub> ) <sub>4</sub> Ar	1132	799	750 (66.3%)	[244]
Sn(O)-C <sub>x</sub> H <sub>y</sub> Sn(C <sub>4</sub> H <sub>9</sub> ) <sub>4</sub> Ar	1553	918	783 (50.4%)	[214,244]; VC addition into electrolyte

In this targeted material development task, the synthesis parameters, mainly the precursor in use, the selected reactive, respectively plasma gas and the microwave power are the key elements for the successful improvement of long-term properties. As explained in Section 4.3.1, and shown by reactions (3–5), a broad variety of material compositions can be realized. It was shown, that increasing the microwave power yields in “cleaner” SnO<sub>2</sub> particles with less precursor residual [60]. Increasing the content of conducting phase (e.g., hydrocarbons) improved the long-term behavior of the anode materials [60]. The use of Ar as plasma gas (according to reaction 6) yields an even better battery performance. This is due to the high amount of carbonaceous phase and its relatively high hydrogen/carbon ratio [214]. Hydrocarbons are known to exhibit very high specific capacities [245–248]. The results are shown in Table 9. It can be seen, that improving battery performance is not only a question of materials properties; also electrode assembly and the selected electrolyte play an important role.

## 6. Summary

Microwave plasma synthesis of particulate matter can be regarded as a subset of diverse plasma reactions, which themselves can be considered as a subset of gas phase reactions. Although several groups are working world-wide successfully in the field of synthesizing all kind of nanomaterials using microwave plasma synthesis methods, a real implementation of laboratory equipment into an industrial process with significant production rates seems not observable to the authors best knowledge. The physico-chemical processes of particle formation in microwave plasmas are not fully understood so far and hinders to some extent up-scaling to industrial relevant production output. One additional bottle neck is the collection of particles with sizes < 5 nm.

Nevertheless, the scientific relevance is given, as synthesized particles may be very small (often with sizes below 5 nm), particle size distributions are narrow, and particles with size-dependent properties, featuring real “nano-effects”, can be synthesized. Literature reveals a broad palette of different materials such as oxides, nitrides, carbides, chalcogenides, carbon materials, metals, composites, and doped particles. Additionally, synthesis of core/shell nanoparticles is possible comprising combined material properties. The process parameters can be used to influence the resulting product, respectively, its properties.

Exemplarily, superparamagnetic, nanosized Fe<sub>2</sub>O<sub>3</sub> particles, different ceramic core/organic shell nanoparticles, and Sn-based composites have been discussed with respect to their properties and application potential.

### Conflicts of Interest

The authors declare no conflict of interest.

### Author Contributions

Dorothee Vinga Szabó designed the concept of the paper. Sabine Schlabach contributed with expert knowledge. The manuscript was written through contributions of both authors. Both authors have given their approval to the final version of the manuscript.

### References

1. Siegel, R.W.; Ramasamy, S.; Hahn, H.; Zongquan, L.; Ting, L.; Gronsky, R. Synthesis, characterization, and properties of nanophase TiO<sub>2</sub>. *J. Mater. Res.* **1988**, *3*, 1367–1372.
2. Gurav, A.; Kodas, T.; Pluym, T.; Xiong, Y. Aerosol Processing of Materials. *Aerosol Sci. Tech.* **1993**, *19*, 411–452.
3. Pratsinis, S.E.; Vemury, S. Particle formation in gases: A review. *Powder Technol.* **1996**, *88*, 267–273.
4. Hahn, H. Gas phase synthesis of nanocrystalline materials. *Nanostruct. Mater.* **1997**, *9*, 3–12.
5. Chen, Y.; Glumac, N.; Kear, B.H.; Skandan, G. High rate synthesis of nanophase materials. *Nanostruct. Mater.* **1997**, *9*, 101–104.
6. Kear, B.H.; Glumac, N.G.; Chen, Y.J.; Skandan, G. Flame Synthesis of Nanophase Oxide Powders. *Part. Sci. Technol.* **1997**, *15*, 174.
7. Skandan, G.; Chen, Y.J.; Glumac, N.; Kear, B.H. Synthesis of oxide nanoparticles in low pressure flames. *Nanostruct. Mater.* **1999**, *11*, 149–158.
8. Rellinghaus, B.; Lindackers, D.; Köckerling, M.; Roth, P.; Wassermann, E.F. The Process of Particle Formation in the Flame Synthesis of Tin Oxide Nanoparticles. *Phase Transit.* **2003**, *76*, 347–354.
9. Vollath, D. Plasma synthesis of nanopowders. *J. Nanopart. Res.* **2008**, *10*, 39–57.
10. Wiggers, H. Novel Material Properties Based on Flame-synthesized Nanomaterials. *KONA* **2009**, 186–194.

11. Kumfer, B.M.; Shinoda, K.; Jeyadevan, B.; Kennedy, I.M. Gas-phase flame synthesis and properties of magnetic iron oxide nanoparticles with reduced oxidation state. *J. Aerosol. Sci.* **2010**, *41*, 257–265.
12. Pratsinis, S.E. Aerosol-based technologies in nanoscale manufacturing: from functional materials to devices through core chemical engineering. *AiChE J.* **2010**, *56*, 3028–3035.
13. Schwade, B.; Roth, P. Simulation of nano-particle formation in a wall-heated aerosol reactor including coalescence. *J. Aerosol. Sci.* **2003**, *34*, 339–357.
14. Giesen, B.; Orthner, H.R.; Kowalik, A.; Roth, P. On the interaction of coagulation and coalescence during gas-phase synthesis of Fe-nanoparticle agglomerates. *Chem. Eng. Sci.* **2004**, *59*, 2201–2211.
15. Paur, H.R.; Baumann, W.; Mätzing, H.; Seifert, H. Formation of nanoparticles in flames; measurement by particle mass spectrometry and numerical simulation. *Nanotechnology* **2005**, *16*, S354–S361.
16. Bosisio, R.G.; Wertheimer, M.R.; Weissfloch, C.F. Generation of large volume microwave plasmas. *J. Phys. E* **1973**, *6*, 628–630.
17. Tonks, L.; Langmuir, I. Oscillations in Ionized Gases. *Phys. Rev.* **1929**, *33*, 195–210.
18. Seiji, S.; Masaru, H.; Shahid, R.; Kunihide, T.; Peter, B.; Gerrit, K.; Whitehead, J.C.; Anthony, B.M.; Alexander, F.G.; Svetlana, S.; *et al.* The 2012 Plasma Roadmap. *J. Phys. D* **2012**, *45*, 253001.
19. Mac Donald, A.D. *Microwave Breakdown in Gases*; John Wiley and Sons: New York, NY, USA, 1966.
20. Kortshagen, U. Nonthermal plasma synthesis of semiconductor nanocrystals. *J. Phys. D* **2009**, *42*, 113001.
21. Szabó, D.V. Microwave Plasma Synthesis of Nanoparticles: From Theoretical Background and Experimental Realization to Nanoparticles with Special Properties. In *Microwaves in Nanoparticle Synthesis: Fundamentals and Applications*; Horikoshi, S., Serpone, N., Eds.; Wiley-VCH: Weinheim, Germany, 2013; pp. 271–309.
22. Tendero, C.; Tixier, C.; Tristant, P.; Desmaison, J.; Leprince, P. Atmospheric pressure plasmas: A review. *Spectrosc. Acta Part B* **2006**, *61*, 2–30.
23. Suzuki, K.; Okudaira, S.; Sakudo, N.; Kanomata, I. Microwave Plasma Etching. *Jpn. J. Appl. Phys.* **1977**, *16*, 1979–1984.
24. Suzuki, K.; Okudaira, S.; Kanomata, I. The Roles of Ions and Neutral Active Species in Microwave Plasma Etching. *J. Electrochem. Soc.* **1979**, *126*, 1024–1028.
25. Suzuki, K.; Okudaira, S.; Nishimatsu, S.; Usami, K.; Kanomata, I. Microwave Plasma Etching of Si with CF<sub>4</sub> and SF<sub>6</sub> Gas. *J. Electrochem. Soc.* **1982**, *129*, 2764–2769.
26. Eddy Jr, C.R.; Sartwell, B.D.; Youchison, D.L. Diamond thin film growth on silicon at temperatures between 500 and 600 °C using an electron cyclotron resonance microwave plasma source. *Surf. Coat. Technol.* **1991**, *48*, 69–79.
27. Szekely, J. Overview of Plasma Processing. *Mat. Res. Soc. Symp. Proc.* **1984**, *30*, 1–11.
28. Young, R.M.; Pfender, E. Generation and behavior of fine particles in thermal plasmas—A review. *Plasma Chem. Plasma Process.* **1985**, *5*, 1–37.

29. Amouroux, J.; Morvan, D.; Gicquel, A. Plasma for special applications. *Fresen. Z. Anal. Chem.* **1986**, 324, 384–396.
30. Chang, Y.; Pfender, E. Thermochemistry of thermal plasma chemical reactions. Part 1. General rules for the prediction of products. *Plasma Chem. Plasma Process.* **1987**, 7, 275–297.
31. Chang, Y.; Young, R.M.; Pfender, E. Thermochemistry of thermal plasma chemical reactions. Part 2. A survey of synthesis routes for silicon nitride production. *Plasma Chem. Plasma Process.* **1987**, 7, 299–316.
32. Moisan, M.; Wertheimer, M.R. Comparison of Microwave and r.f. Plasmas: Fundamentals and Applications. *Surf. Coat. Technol.* **1993**, 59, 1–13.
33. Kamo, M.; Sato, Y.; Matsumoto, S.; Setaka, N. Diamond synthesis from gas phase in microwave plasma. *J. Cryst. Growth* **1983**, 62, 642–644.
34. Saito, Y.; Matsuda, S.; Nogita, S. Synthesis of diamond by decomposition of methane in microwave plasma. *J. Mater. Sci. Lett.* **1986**, 5, 565–568.
35. Saito, Y.; Sato, K.; Tanaka, H.; Fujita, K.; Matuda, S. Diamond synthesis from methane-hydrogen-water mixed gas using a microwave plasma. *J. Mater. Sci.* **1988**, 23, 842–846.
36. Takagi, H.; Ogawa, H.; Yamazaki, Y.; Ishizaki, A.; Nakagiri, T. Quantum size effects on photoluminescence in ultrafine Si particles. *Appl. Phys. Lett.* **1990**, 56, 2379–2380.
37. Mehta, P.; Singh, A.K.; Kingon, A.I. Nonthermal Microwave Plasma Synthesis of Crystalline Titanium Oxide and Titanium Nitride Nanoparticles. *Mat. Res. Soc. Symp. Proc.* **1992**, 249, 153–159.
38. Sickafus, K.E.; Vollath, D.; Varma, R. Electron-Microscopy Study on Zirconia and Alumina Ceramic Powders Synthesized by Microwave Plasma Pyrolysis. *Mat. Res. Soc. Symp. Proc.* **1992**, 269, 363–369.
39. Vollath, D.; Varma, R.; Sickafus, K.E. Synthesis of Nanocrystalline Powders for Oxide Ceramics by Microwave Plasma Pyrolysis. *Mat. Res. Soc. Symp. Proc.* **1992**, 269, 379–384.
40. Chou, C.H.; Phillips, J. Plasma production of metallic nanoparticles. *J. Mater. Res.* **1992**, 7, 2107–2113.
41. Vollath, D.; Sickafus, K.E. Synthesis of nanosized ceramic oxide powders by microwave plasma reactions. *Nanostruct. Mater.* **1992**, 1, 427–437.
42. Vollath, D.; Sickafus, K.E. Synthesis of Ceramic Oxide Powders by Microwave Plasma Pyrolysis. *J. Mater. Sci.* **1993**, 28, 5943–5948.
43. Vollath, D.; Sickafus, K.E. Synthesis of Ceramic Oxide Powders in a Microwave Plasma-Device. *J. Mater. Res.* **1993**, 8, 2978–2984.
44. Vollath, D.; Szabó, D.V. Nanocoated particles: A special type of ceramic powder. *Nanostruct. Mater.* **1994**, 4, 927–938.
45. Brenner, J.R.; Harkness, J.B.L.; Knickelbein, M.B.; Krumdick, G.K.; Marshall, C.L. Microwave plasma synthesis of carbon-supported ultrafine metal particles. *Nanostruct. Mater.* **1997**, 8, 1–17.
46. Aliev, Y.M.; Maximov, A.V.; Kortshagen, U.; Schlüter, H.; Shivarova, A. Modeling of microwave discharges in the presence of plasma resonances. *Phys. Rev. E* **1995**, 51, 6091–6103.
47. Kortshagen, U.; Bhandarkar, U. Modeling of particulate coagulation in low pressure plasmas. *Phys. Rev. E* **1999**, 60, 887–898.

48. Janzen, C.; Kleinwechter, H.; Knipping, J.; Wiggers, H.; Roth, P. Size analysis in low-pressure nanoparticle reactors: comparison of particle mass spectrometry with *in situ* probing transmission electron microscopy. *J. Aerosol. Sci.* **2002**, *33*, 833–841.
49. Giesen, B.; Wiggers, H.; Kowalik, A.; Roth, P. Formation of Si-nanoparticles in a microwave reactor: Comparison between experiments and modelling. *J. Nanopart. Res.* **2005**, *7*, 29–41.
50. Gatti, M.; Kortshagen, U. Analytical model of particle charging in plasmas over a wide range of collisionality. *Phys. Rev. E* **2008**, *78*, 046402.
51. Vollath, D.; Lamparth, I.; Szabó, D.V. Fluorescence from coated oxide nanoparticles. *Mat. Res. Soc. Symp. Proc.* **2002**, *703*, 03–308.
52. Li, S.-Z.; Hong, Y.C.; Uhm, H.S.; Li, Z.-K. Synthesis of Nanocrystalline Iron Oxide Particles by Microwave Plasma Jet at Atmospheric Pressure. *Jpn. J. Appl. Phys.* **2004**, *43*, 7714–7717.
53. Schumacher, B.; Ochs, R.; Tröbe, H.; Schlabach, S.; Bruns, M.; Szabo, D.V.; Haußelt, J. Electronic micro nose equipped with nano-structured gas sensitive SnO<sub>2</sub>. *MST News* **2006**, *6*, 10–12.
54. Schumacher, B.; Ochs, R.; Tröbe, H.; Schlabach, S.; Bruns, M.; Szabó, D.V.; Haußelt, J. Nanogranular SnO<sub>2</sub> Layers for Gas Sensing Applications by In Situ Deposition of Nanoparticles Produced by the Karlsruhe Microwave Plasma Process. *Plasma Process. Polym.* **2007**, *4*, S865–S870.
55. Mahendra Kumar, S.; Deshpande, P.A.; Krishna, M.; Krupashankara, M.S.; Madras, G. Photocatalytic Activity of Microwave Plasma-Synthesized TiO<sub>2</sub> Nanopowder. *Plasma Chem. Plasma Process.* **2010**, *30*, 461–470.
56. Hong, Y.C.; Lho, T.; Lee, B.J.; Uhm, H.S.; Kwon, O.P.; Lee, S.H. Synthesis of titanium dioxide in O<sub>2</sub>/Ar/SO<sub>2</sub>/TiCl<sub>4</sub> microwave torch plasma and its band gap narrowing. *Curr. Appl. Phys.* **2011**, *11*, 517–520.
57. Kautsch, A.; Brossmann, U.; Krenn, H.; Hofer, F.; Szabó, D.V.; Würschum, R. Structural and optical properties of nanoparticulate Y<sub>2</sub>O<sub>3</sub>:Eu<sub>2</sub>O<sub>3</sub> made by microwave plasma synthesis. *Appl. Phys. A* **2011**, *105*, 709–712.
58. Nadeem, K.; Krenn, H.; Traussnig, T.; Würschum, R.; Szabó, D.V.; Letofsky-Papst, I. Effect of dipolar and exchange interactions on magnetic blocking of maghemite nanoparticles. *J. Magn. Magn. Mat.* **2011**, *323*, 1998–2004.
59. Petermann, N.; Stein, N.; Schierning, G.; Theissmann, R.; Stoib, B.; Brandt, M.S.; Hecht, C.; Schulz, C.; Wiggers, H. Plasma synthesis of nanostructures for improved thermoelectric properties. *J. Phys. D* **2011**, *44*, 174034.
60. Szabó, D.V.; Kilibarda, G.; Schlabach, S.; Trouillet, V.; Bruns, M. Structural and chemical characterization of SnO<sub>2</sub>-based nanoparticles as electrode material in Li-ion batteries. *J. Mater. Sci.* **2012**, *47*, 4383–4391.
61. Ishigaki, T. Synthesis of ceramic nanoparticles with non-equilibrium crystal structures and chemical compositions by controlled thermal plasma processing. *J. Ceram. Soc. Jpn.* **2008**, *116*, 462–470.
62. Schütze, A.; Jeong, J.Y.; Babayan, S.E.; Park, J.; Selwyn, G.S.; Hicks, R.F. The atmospheric-pressure plasma jet: A review and comparison to other plasma sources. *IEEE Trans. Plasma Sci.* **1998**, *26*, 1685–1694.

63. Phillips, J.; Luhrs, C.C.; Richard, M. Review: Engineering Particles Using the Aerosol-Through-Plasma Method. *IEEE Trans. Plasma Sci.* **2009**, *37*, 726–739.
64. Bárdos, L.; Baránková, H. Cold atmospheric plasma: Sources, processes, and applications. *Thin Solid Films* **2010**, *518*, 6705–6713.
65. Belmonte, T.; Arnoult, G.; Henrion, G.; Gries, T. Nanoscience with non-equilibrium plasmas at atmospheric pressure. *J. Phys. D* **2011**, *44*, 363001.
66. Vollath, D. *Nanomaterials: An Introduction to Synthesis, Properties and Applications*, 1st ed.; Wiley-VCH: Weinheim, Germany, 2008.
67. Vollath, D. Estimation of particle size distributions obtained by gas phase processes. *J. Nanopart. Res.* **2011**, *13*, 3899–3909.
68. Schweigert, V.A.; Schweigert, I.V. Coagulation in a low-temperature plasma. *J. Phys. D* **1996**, *29*, 655–659.
69. Kortshagen, U.R.; Bhandarkar, U.V.; Swihart, M.T.; Girshick, S.L. Generation and growth of nanoparticles in low-pressure plasmas. *Pure Appl. Chem.* **1999**, *71*, 1871–1877.
70. Mangolini, L.; Kortshagen, U. Selective nanoparticle heating: Another form of nonequilibrium in dusty plasmas. *Phys. Rev. E* **2009**, *79*, 026405.
71. Galli, F.; Kortshagen, U.R. Charging, Coagulation, and Heating Model of Nanoparticles in a Low-Pressure Plasma Accounting for Ion-Neutral Collisions. *IEEE Trans. Plasma Sci.* **2010**, *38*, 803–809.
72. Janzen, C.; Wiggers, H.; Knipping, J.; Roth, P. Formation and *in situ* sizing of gamma-Fe<sub>2</sub>O<sub>3</sub> nanoparticles in a microwave flow reactor. *J. Nanosci. Nanotech.* **2001**, *1*, 221–225.
73. Kleinwechter, H.; Janzen, C.; Knipping, J.; Wiggers, H.; Roth, P. Formation and properties of ZnO nanoparticles from gas-phase synthesis processes. *J. Mater. Sci.* **2002**, *37*, 4349–4360.
74. Vollath, D.; Szabó, D.V. The Microwave plasma process—A versatile process to synthesise nanoparticulate materials. *J. Nanopart. Res.* **2006**, *8*, 417–428.
75. Baumann, W.; Thekedar, B.; Paur, H.R.; Seifert, H. Characterization of nanoparticles synthesized in the microwave plasma discharge process by particle mass spectrometry and transmission electron microscopy. In Proceedings of AiChE Fall and Annual Meeting, San Francisco, CA, USA, 12–17 November 2006.
76. Baumann, W.; Thekedar, B.; Paur, H.R.; Seifert, H. Comparison of size distribution of iron oxide nanoparticles measured with particle mass spectrometer and transmission electron microscopy. In Proceedings of International Congress on Particle Technology (PARTEC 2007), Nürnberg, Germany, 27–29 March 2007.
77. Gozum, J.E.; Pollina, D.M.; Jensen, J.A.; Girolami, G.S. “Tailored” organometallics as precursors for the chemical vapor deposition of high-purity palladium and platinum thin films. *J. Am. Chem. Soc.* **1988**, *110*, 2688–2689.
78. Hampden-Smith, M.J.; Kodas, T.T. Chemical vapor deposition of metals: Part 1. An overview of CVD processes. *Chem. Vap. Depos.* **1995**, *1*, 8–23.
79. Rossetto, G.; Zanella, P.; Carta, G.; Bertani, R.; Favretto, D.; Ingo, G.M. Synthesis and characterization of methylcyclopentadienyl-( $\eta^3$ -allyl)platinum and its use as a metallo-organic chemical vapour deposition precursor of platinum. *Appl. Organomet. Chem.* **1999**, *13*, 509–513.

80. Thekedar, B. Size characterization of nanoparticles synthesized in microwave plasma discharge process. Master Thesis, University of Magdeburg, Chemical and Process Engineering, Magdeburg, Germany, February 2006.
81. Knipping, J.; Wiggers, H.; Rellinghaus, B.; Roth, P.; Konjhodzic, D.; Meier, C. Synthesis of high purity silicon nanoparticles in a low pressure microwave reactor. *J. Nanosci. Nanotech.* **2004**, *4*, 1039–1044.
82. Shimada, M.; Wang, W.-N.; Okuyama, K. Synthesis of Gallium Nitride Nanoparticles by Microwave Plasma-Enhanced CVD. *Chem. Vap. Depos.* **2010**, *16*, 151–156.
83. Szabó, D.V.; Schlabach, S.; Ochs, R. Analytical TEM investigations of size effects in SnO<sub>2</sub> nanoparticles produced by microwave plasma synthesis. *Microsc. Microanal.* **2007**, *13*, 430–431.
84. Vennekamp, M.; Bauer, I.; Groh, M.; Sperling, E.; Ueberlein, S.; Myndyk, M.; Mäder, G.; Kaskel, S. Formation of SiC nanoparticles in an atmospheric microwave plasma. *Beilstein J. Nanotechnol.* **2011**, *2*, 665–673.
85. Fu, L.; Johnson, D.L.; Zheng, J.G.; Dravid, V.P. Microwave Plasma Synthesis of Nanostructured  $\gamma$ -Al<sub>2</sub>O<sub>3</sub> Powders. *J. Am. Ceram. Soc.* **2003**, *86*, 1635–1637.
86. Schlabach, S.; Szabó, D.V.; Shi, Z.; Wang, D.; Vollath, D. Synthesis of nanoparticulate SiC in a low temperature microwave plasma process. In *Nanofair 2004: New Ideas for Industry*; VDI-Berichte: Karlsruhe, Germany, 2004; pp. 167–170.
87. Vollath, D.; Szabó, D.V.; Hausselet, J. Synthesis and properties of ceramic nanoparticles and nanocomposites. *J. Europ. Ceram. Soc.* **1997**, *17*, 1317–1324.
88. Mühleisen, M.; Möbius, A. Vorrichtung zur reflektionsarmen Absorption von Mikrowellen. Patent DE 195 28 343 C2, May 1997.
89. Vollath, D.; Szabó, D.V. Synthesis of nanopowders by the microwave plasma process—basic considerations and perspectives for scaling up. In *Innovative Processing of Films and Nanocrystalline Powders*, 1st ed.; Choy, K.-L., Ed.; Imperial College Press: London, UK, 2002; pp. 219–251.
90. Zheng, F. Thermophoresis of spherical and non-spherical particles: A review of theories and experiments. *Adv. Colloid Interface Sci.* **2002**, *97*, 255–278.
91. Piazza, R. Thermophoresis: Moving particles with thermal gradients. *Soft Matter* **2008**, *4*, 1740–1744.
92. Abdali, A.; Moritz, B.; Gupta, A.; Wiggers, H.; Schulz, C. Hybrid microwave-plasma hot-wall reactor for synthesis of silica nanoparticles under well-controlled conditions. *J. Optoelectron. Adv. Mater.* **2010**, *12*, 440–444.
93. Tsai, C.-J.; Chen, S.-C.; Przekop, R.; Moskal, A. Study of an Axial Flow Cyclone to Remove Nanoparticles in Vacuum. *Environ. Sci. Technol.* **2007**, *41*, 1689–1695.
94. Chen, S.-C.; Tsai, C.-J. An axial flow cyclone to remove nanoparticles at low pressure conditions. *J. Nanopart. Res.* **2007**, *9*, 71–83.
95. Girshick, S.L.; Chiu, C.P.; Munro, R.; Wu, C.Y.; Yang, L.; Singh, S.K.; McMurry, P.H. Thermal plasma synthesis of ultrafine iron particles. *J. Aerosol. Sci.* **1993**, *24*, 367–382.
96. Krinke, T.J.; Deppert, K.; Magnusson, M.H.; Schmidt, F.; Fissan, H. Microscopic aspects of the deposition of nanoparticles from the gas phase. *J. Aerosol. Sci.* **2002**, *33*, 1341–1359.

97. Sagmeister, M.; Brossmann, U.; List, E.J.W.; Ochs, R.; Szabó, D.V.; Würschum, R. *In-situ* dispersion of ZrO<sub>2</sub> nano-particles coated with pentacene. *Phys. Status Solidi RRL* **2008**, *2*, 203–205.
98. Schlabach, S.; Ochs, R.; Hanemann, T.; Szabó, D.V. Nanoparticles in polymer-matrix composites. *Microsyst. Technol.* **2011**, *17*, 183–193.
99. Schumacher, B.; Szabó, D.V.; Schlabach, S.; Ochs, R.; Müller, H.; Bruns, M. Nanoparticle SnO<sub>2</sub> films as gas sensitive membranes. *Mat. Res. Soc. Symp. Proc.* **2006**, *900E*, O08 06.01—O08 06.06.
100. Ochs, R.; Szabó, D.V.; Schlabach, S.; Becker, S.; Indris, S. Development of nanocomposites for anode materials in Li-ion batteries. *Phys. Status Solidi A* **2011**, *208*, 471–473.
101. Kalyanaraman, R.; Yoo, S.; Krupashankara, M.S.; Sudarshan, T.S.; Dowding, R.J. Synthesis and consolidation of iron nanopowders. *Nanostruct. Mater.* **1998**, *10*, 1379–1392.
102. David, B.; Pizúrová, N.; Schneeweiss, O.; Šantavá, E.; Kudrle, V.; Jašek, O.  $\gamma$ -Fe<sub>2</sub>O<sub>3</sub> nanopowders synthesized in microwave plasma and extraordinarily strong temperature influence on their Mössbauer spectra. *J. Nanosci. Nanotech.* **2012**, *12*, 9277–9285.
103. David, B.; Pizúrová, N.; Synek, P.; Kudrle, V.; Jašek, O.; Schneeweiss, O.  $\epsilon$ -Fe<sub>2</sub>O<sub>3</sub> nanoparticles synthesized in atmospheric-pressure microwave torch. *Mater. Lett.* **2014**, *116*, 370–373.
104. Bywalez, R.; Karacuban, H.; Nienhaus, H.; Schulz, C.; Wiggers, H. Stabilization of mid-sized silicon nanoparticles by functionalization with acrylic acid. *Nanoscale Res. Lett.* **2012**, *7*, 76.
105. Nadeem, K.; Krenn, H.; Traußnig, T.; Würschum, R.; Szabó, D.V.; Letofsky-Papst, I. Spin-glass freezing of maghemite nanoparticles prepared by microwave plasma synthesis. *J. Appl. Phys.* **2012**, *111*, 113911.
106. Vollath, D.; Szabó, D.V. Microwave plasma synthesis of ceramic nanopowders. *J. Aerosol. Sci.* **1997**, *28*, S685–S688.
107. Vollath, D.; Szabó, D.V.; Taylor, R.D.; Willis, J.O.; Sickafus, K.E. Synthesis and properties of nanocrystalline superparamagnetic gamma-Fe<sub>2</sub>O<sub>3</sub>. *Nanostruct. Mater.* **1995**, *6*, 941–944.
108. Vollath, D.; Szabó, D.V.; Taylor, R.D.; Willis, J.O. Synthesis and magnetic properties of nanostructured maghemite. *J. Mater. Res.* **1997**, *12*, 2175–2182.
109. David, B.; Schneeweiss, O.; Šantavá, E.; Jašek, O. Magnetic properties of  $\gamma$ -Fe<sub>2</sub>O<sub>3</sub> nanopowder synthesized by atmospheric microwave torch discharge. *Acta Phys. Pol. A* **2012**, *122*, 9–11.
110. Synek, P.; Jašek, O.; Zajíčková, L.; David, B.; Kudrle, V.; Pizúrová, N. Plasmachemical synthesis of maghemite nanoparticles in atmospheric pressure microwave torch. *Mater. Lett.* **2011**, *65*, 982–984.
111. Synek, P.; Jašek, O.; Zajíčková, L. Study of Microwave Torch Plasmachemical Synthesis of Iron Oxide Nanoparticles Focused on the Analysis of Phase Composition. *Plasma Chem. Plasma Process.* **2014**, *34*, 327–341.
112. Son, S.; Taheri, M.; Carpenter, E.; Harris, V.G.; McHenry, M.E. Synthesis of ferrite and nickel ferrite nanoparticles using radio-frequency thermal plasma torch. *J. Appl. Phys.* **2002**, *91*, 7589–7591.
113. Vissokov, G.P.; Pirgov, P.S. Plasma-chemical synthesis of ultradispersed iron oxides with pigment qualification. *J. Mater. Sci.* **1996**, *31*, 4007–4016.

114. Banerjee, I.; Kholam, Y.B.; Balasubramanian, C.; Pasricha, R.; Bakare, P.P.; Patil, K.R.; Das, A.K.; Bhoraskar, S.V. Preparation of  $\gamma$ -Fe<sub>2</sub>O<sub>3</sub> nanoparticles using DC thermal arc-plasma route, their characterization and magnetic properties. *Scr. Mater.* **2006**, *54*, 1235–1240.
115. Lei, P.; Boies, A.; Calder, S.; Girshick, S. Thermal Plasma Synthesis of Superparamagnetic Iron Oxide Nanoparticles. *Plasma Chem. Plasma Process.* **2012**, *32*, 519–531.
116. Brossmann, U.; Sagmeister, M.; Polt, P.; Kothleitner, G.; Letofsky-Papst, I.; Szabó, D.V.; Würschum, R. Microwave plasma synthesis of nano-crystalline YSZ. *Phys. Status Solidi RRL* **2007**, *1*, 107–109.
117. Forker, M.; Schmidberger, J.; Szabó, D.V.; Vollath, D. Perturbed-angular-correlation study of phase transformations in nanoscaled Al<sub>2</sub>O<sub>3</sub>-coated and noncoated ZrO<sub>2</sub> particles synthesized in a microwave plasma. *Phys. Rev. B* **2000**, *61*, 1014–1025.
118. Schlabach, S.; Szabó, V.; Vollath, D.; Braun, A.; Clasen, R. Structure of alumina and zirconia nanoparticles synthesized by the Karlsruhe Microwave Plasma Process. *Solid State Phenom.* **2004**, *99–100*, 191–196.
119. Forker, M.; de la Presa, P.; Hoffbauer, W.; Schlabach, S.; Bruns, M.; Szabó, D.V. Structure, phase transformations, and defects of HfO<sub>2</sub> and ZrO<sub>2</sub> nanoparticles studied by Ta-<sup>181</sup> and Cd-<sup>111</sup> perturbed angular correlations, H-<sup>1</sup> magic-angle spinning NMR, XPS, and X-ray and electron diffraction. *Phys. Rev. B* **2008**, *77*, 054108.
120. Schlabach, S.; Szabó, D.V.; Vollath, D.; de la Presa, P.; Forker, M. Zirconia and titania nanoparticles studied by electric hyperfine interactions, XRD and TEM. *J. Alloy. Compd.* **2007**, *434*, 590–593.
121. Ye, R.; Li, J.G.; Ishigaki, T. Controlled synthesis of alumina nanoparticles using inductively coupled thermal plasma with enhanced quenching. *Thin Solid Films* **2007**, *515*, 4251–4257.
122. Szabó, D.V.; Kilibarda, G.; Schlabach, S. Microwave plasma synthesis of nanomaterials for Li-ion battery application. In *13th International Conference on Microwave and High Frequency Heating (AMPERE 2011)*; Tao, J., Ed.; CEPAD: Toulouse, France, 2011; pp. 425–428.
123. Im, J.-H.; Lee, J.-H.; Park, D.-W. Synthesis of nano-sized tin oxide powder by argon plasma jet at atmospheric pressure. *Surf. Coat. Technol.* **2008**, *202*, 5471–5475.
124. Schlabach, S.; Szabó, D.V.; Vollath, D.; de la Presa, P.; Forker, M. Structure and grain growth of TiO<sub>2</sub> nanoparticles investigated by electron and X-ray diffractions and Ta-<sup>181</sup> perturbed angular correlations. *J. Appl. Phys.* **2006**, *100*, 024305.
125. Hong, Y.C.; Bang, C.U.; Shin, D.H.; Uhm, H.S. Band gap narrowing of TiO<sub>2</sub> by nitrogen doping in atmospheric microwave plasma. *Chem. Phys. Lett.* **2005**, *413*, 454–457.
126. Hong, Y.C.; Uhm, H.S. Production of nanocrystalline TiO<sub>2</sub> powder by a microwave plasma-torch and its characterization. *Jpn. J. Appl. Phys.* **2007**, *46*, 6027–6031.
127. Oh, S.-M.; Li, J.-G.; Ishigaki, T. Nanocrystalline TiO<sub>2</sub> powders synthesized by in-flight oxidation of TiN in thermal plasma: Mechanisms of phase selection and particle morphology evolution. *J. Mater. Res.* **2005**, *20*, 529–537.
128. Wangenstein, T.; Dhakal, T.; Merlak, M.; Mukherjee, P.; Phan, M.H.; Chandra, S.; Srikanth, H.; Witanachchi, S. Growth of uniform ZnO nanoparticles by a microwave plasma process. *J. Alloy. Compd.* **2011**, *509*, 6859–6863.

129. Hong, Y.C.; Kim, J.H.; Cho, S.C.; Uhm, H.S. ZnO nanocrystals synthesized by evaporation of Zn in microwave plasma torch in terms of mixture ratio of N<sub>2</sub> to O<sub>2</sub>. *Phys. Plasmas* **2006**, *13*, 063506.
130. Kim, J.H.; Hong, Y.C.; Uhm, H.S. Synthesis of oxide nanoparticles via microwave plasma decomposition of initial materials. *Surf. Coat. Technol.* **2007**, *201*, 5114–5120.
131. Sato, T.; Tanigaki, T.; Suzuki, H.; Saito, Y.; Kido, O.; Kimura, Y.; Kaito, C.; Takeda, A.; Kaneko, S. Structure and optical spectrum of ZnO nanoparticles produced in RF plasma. *J. Cryst. Growth* **2003**, *255*, 313–316.
132. Felbier, P.; Yang, J.; Theis, J.; Liptak, R.W.; Wagner, A.; Lorke, A.; Bacher, G.; Kortshagen, U. Highly Luminescent ZnO Quantum Dots Made in a Nonthermal Plasma. *Adv. Funct. Mater.* **2014**, *24*, 1988–1993.
133. Vollath, D.; Szabó, D.V.; Willis, J.O. Magnetic properties of nanocrystalline Cr<sub>2</sub>O<sub>3</sub> synthesized in a microwave plasma. *Mater. Lett.* **1996**, *29*, 271–279.
134. Cho, S.C.; Hong, Y.C.; Uhm, H.S. TeO<sub>2</sub> nanoparticles synthesized by evaporation of tellurium in atmospheric microwave-plasma torch-flame. *Chem. Phys. Lett.* **2006**, *429*, 214–218.
135. Hong, Y.C.; Uhm, H.S. Synthesis of MgO nanopowder in atmospheric microwave plasma torch. *Chem. Phys. Lett.* **2006**, *422*, 174–178.
136. Shin, D.H.; Bang, C.U.; Hong, Y.C.; Uhm, H.S. Preparation of vanadium pentoxide powders by microwave plasma-torch at atmospheric pressure. *Mater. Chem. Phys.* **2006**, *99*, 269–275.
137. Sagmeister, M.; Postl, M.; Brossmann, U.; List, E.J.E.; Klug, A.; Letofsky-Papst, I.; Szabó, D.V.; Würschum, R. Structure and electrical properties of nanoparticulate tungsten oxide prepared by microwave plasma synthesis. *J. Phys.* **2011**, *23*, 334206.
138. Su, C.-Y.; Lin, C.-K.; Yang, T.-K.; Lin, H.-C.; Pan, C.-T. Oxygen partial pressure effect on the preparation of nanocrystalline tungsten oxide powders by a plasma arc gas condensation technique. *Int. J. Refract. Met. Hard Mat.* **2008**, *26*, 423–428.
139. Anthony, R.; Thimsen, E.; Johnson, J.; Campbell, S.; Kortshagen, U. A non-thermal plasma reactor for the synthesis of Gallium Nitride nanocrystals. *Mat. Res. Soc. Symp. Proc.* **2006**, *892*, 221–224.
140. Shimada, M.; Azuma, Y.; Okuyama, K.; Hayashi, Y.; Tanabe, E. Plasma synthesis of light emitting gallium nitride nanoparticles using a novel microwave-resonant cavity. *Jpn. J. Appl. Phys.* **2006**, *45*, 328–332.
141. Shin, D.H.; Hong, Y.C.; Uhm, H.S. Production of Nanocrystalline Titanium Nitride Powder by Atmospheric Microwave Plasma Torch in Hydrogen/Nitrogen Gas. *J. Am. Ceram. Soc.* **2005**, *88*, 2736–2739.
142. Bang, C.U.; Hong, Y.C.; Uhm, H.S. Synthesis and characterization of nano-sized nitride particles by using an atmospheric microwave plasma technique. *Surf. Coat. Technol.* **2007**, *201*, 5007–5011.
143. Kumar, S.; Murugan, K.; Chandrasekhar, S.B.; Hebalkar, N.; Krishna, M.; Satyanarayana, B.S.; Madras, G. Synthesis and characterization of nano silicon and titanium nitride powders using atmospheric microwave plasma technique. *J. Chem. Sci.* **2012**, *124*, 557–563.
144. Chau, J.L.H.; Kao, C.C. Microwave plasma synthesis of TiN and ZrN nanopowders. *Mater. Lett.* **2007**, *61*, 1583–1587.

145. Yoshida, T.; Kawasaki, A.; Nakagawa, K.; Akashi, K. The synthesis of ultrafine titanium nitride in an r.f. plasma. *J. Mater. Sci.* **1979**, *14*, 1624–1630.
146. Vollath, D.; Sickafus, K.E. Synthesis of nanosized ceramic nitride powders by microwave supported plasma reactions. *Nanostruct. Mater.* **1993**, *2*, 451–456.
147. Vollath, D.; Szabó, D.V. Nanoparticles from compounds with layered structures. *Acta Mater.* **2000**, *48*, 953–967.
148. Hong, Y.C.; Shin, D.H.; Uhm, H.S. Production of vanadium nitride nanopowders from gas-phase  $\text{VOCl}_3$  by making use of microwave plasma torch. *Mater. Chem. Phys.* **2007**, *101*, 35–40.
149. Szepvolgyi, J.; Mohai-Toth, I.; Bertoti, I.; Gilbert, E.; Riley, F.L. Synthesis of silicon nitride powders in an RF plasma torch, and studies of their sintering behaviour. *Key Eng. Mat.* **1994**, *89–91*, 35–40.
150. Baba, K.; Shohata, N.; Yonezawa, M. Synthesis and properties of ultrafine AlN powder by rf plasma. *Appl. Phys. Lett.* **1989**, *54*, 2309–2311.
151. Etemadi, K. Formation of aluminum nitrides in thermal plasmas. *Plasma Chem. Plasma Process.* **1991**, *11*, 41–56.
152. Troitskiy, V.N.; Domashnev, I.A.; Kurkin, E.N.; Grebtsova, O.M.; Berestenko, V.I.; Balikhin, I.L.; Gurov, S.V. Synthesis and Characteristics of Ultra-Fine Superconducting Powders in the Nb–N, Nb–N–C, Nb–Ti–N–C systems. *J. Nanopart. Res.* **2003**, *5*, 521–528.
153. Lin, H.; Gerbec, J.A.; Sushchikh, M.; McFarland, E.W. Synthesis of amorphous silicon carbide nanoparticles in a low temperature low pressure plasma reactor. *Nanotechnology* **2008**, *19*, 325601.
154. Viera, G.; Costa, J.; Roura, P.; Bertran, E. High nucleation rate in pure SiC nanometric powder by a combination of room temperature plasmas and post-thermal treatments. *Diam. Relat. Mat.* **1999**, *8*, 364–368.
155. Andújar, J.L.; Viera, G.; Polo, M.C.; Maniette, Y.; Bertran, E. Synthesis of nanosize Si-C-N powder in low pressure plasmas. *Vacuum* **1999**, *52*, 153–156.
156. Ko, S.M.; Koo, S.M.; Kim, J.H.; Cho, W.S.; Hwang, K.T. Synthesis of silicon carbide nano-powder from a silicon-organic precursor by RF inductive thermal plasma. *J. Korean Ceram. Soc.* **2012**, *49*, 523–527.
157. Hollabaugh, C.M.; Hull, D.E.; Newkirk, L.R.; Petrovic, J.J. RF-plasma system for the production of ultrafine, ultrapure silicon carbide powder. *J. Mater. Sci.* **1983**, *18*, 3190–3194.
158. Kong, P.; Huang, T.T.; Pfender, E. Synthesis of Ultrafine Silicon Carbide Powders in Thermal Arc Plasmas. *IEEE Trans. Plasma Sci.* **1986**, *14*, 357–369.
159. Kong, P.C.; Pfender, E. Formation of ultrafine  $\beta$ -silicon carbide powders in an argon thermal plasma jet. *Langmuir* **1987**, *3*, 259–265.
160. Guo, J.Y.; Gitzhofer, F.; Boulos, M.I. Induction plasma synthesis of ultrafine SiC powders from silicon and  $\text{CH}_4$ . *J. Mater. Sci.* **1995**, *30*, 5589–5599.
161. Allaire, F.; Parent, L.; Dallaire, S. Production of submicron SiC particles by D.C. thermal plasma: A systematic approach based on injection parameters. *J. Mater. Sci.* **1991**, *26*, 4160–4165.
162. Du, S.W.; Tok, A.I.Y.; Boey, F.Y.C. RF plasma synthesis of boron carbide nanoparticles. *Solid State Phenom.* **2008**, *136*, 23–38.

163. Kouprine, A.; Gitzhofer, F.; Boulos, M.; Veres, T. Synthesis of ferromagnetic nanopowders from iron pentacarbonyl in capacitively coupled RF plasma. *Carbon* **2006**, *44*, 2593–2601.
164. Gurentsov, E.; Priemchenko, K.; Grimm, H.; Orthner, H.; Wiggers, H.; Borchers, C.; Jander, H.; Eremin, A.; Schulz, C. Synthesis of Small Carbon Nanoparticles in a Microwave Plasma Flow Reactor. *Z. Phys. Chem.* **2013**, *227*, 357–370.
165. Gries, T.; Vandenbulcke, L.; Rouzaud, J.N.; De Persis, S. Diagnostics in dusty C-H-O plasmas with diamond and graphitic nanoparticle generation. *Plasma Sources Sci. Technol.* **2010**, *19*, 025015.
166. Kovacevic, E.; Berndt, J.; Strunskus, T.; Boufendi, L. Size dependent characteristics of plasma synthesized carbonaceous nanoparticles. *J. Appl. Phys.* **2012**, *112*, 013303.
167. Tian, M.; Batty, S.; Shang, C. Synthesis of nanostructured carbons by the microwave plasma cracking of methane. *Carbon* **2013**, *51*, 243–248.
168. Ting, C.C.; Young, T.F.; Jwo, C.S. Fabrication of diamond nanopowder using microwave plasma torch technique. *Int. J. Adv. Manuf. Tech.* **2007**, *34*, 316–322.
169. Fu, D.J.; Liu, X.G.; Du, A.B.; Han, P.D.; Jia, H.S.; Xu, B.S. Synthesis of nano-structured onion-like fullerenes by MW plasma. *J. Inorg. Mater.* **2006**, *21*, 576–582.
170. Vollath, D.; Szabo, D.V. Synthesis of nanocrystalline MoS<sub>2</sub> and WS<sub>2</sub> in a microwave plasma. *Mater. Lett.* **1998**, *35*, 236–244.
171. Szabó, D.V.; Vollath, D. Morphological characterisation of nanocrystals with layered structures. *Nanostruct. Mater.* **1999**, *12*, 597–600.
172. Brooks, D.J.; Douthwaite, R.E.; Brydson, R.; Calvert, C.; Measures, M.G.; Watson, A. Synthesis of inorganic fullerene (MS<sub>2</sub>, M = Zr, Hf and W) phases using H<sub>2</sub>S and N<sub>2</sub>/H<sub>2</sub> microwave-induced plasmas. *Nanotechnology* **2006**, *17*, 1245–1250.
173. David, B.; Pizúrová, N.; Schneeweiss, O.; Šantavá, E.; Jašek, O.; Kudrle, V.  $\alpha$ -Fe nanopowder synthesised in low-pressure microwave plasma and studied by Mössbauer spectroscopy. *J. Phys. Conf. Ser.* **2011**, *303*, 012090.
174. David, B.; Pizúrová, N.; Schneeweiss, O.; Kudrle, V.; Jašek, O.; Synek, P. Iron-based nanopowders containing  $\alpha$ -Fe, Fe<sub>3</sub>C, and  $\gamma$ -Fe particles synthesised in microwave torch plasma and investigated with Mössbauer spectroscopy. *Jpn. J. Appl. Phys.* **2011**, *50*, 08JF11.
175. Poddar, P.; Wilson, J.L.; Srikanth, H.; Ravi, B.G.; Wachsmuth, J.; Sudarshan, T.S. Grain size influence on soft ferromagnetic properties in Fe–Co nanoparticles. *Mater. Sci. Eng. B* **2004**, *106*, 95–100.
176. Panchal, V.; Lahoti, G.; Bhandarkar, U.; Neergat, M. The effects of process parameters on yield and properties of iron nanoparticles from ferrocene in a low-pressure plasma. *J. Phys. D* **2011**, *44*, 345205.
177. Weigle, J.C.; Luhrs, C.C.; Chen, C.K.; Perry, W.L.; Mang, J.T.; Nemer, M.B.; Lopez, G.P.; Phillips, J. Generation of Aluminum Nanoparticles Using an Atmospheric Pressure Plasma Torch. *J. Phys. Chem. B* **2004**, *108*, 18601–18607.
178. Bertran, E.; Costa, J.; Viera, G.; Zhang, R.Q. Production of nanometric particles in radio frequency glow discharges in mixtures of silane and methane. *J. Vac. Sci. Technol. A* **1996**, *14*, 567–571.

179. Bapat, A.; Perrey, C.R.; Campbell, S.A.; Carter, C.B.; Kortshagen, U. Synthesis of highly oriented, single-crystal silicon nanoparticles in a low-pressure, inductively coupled plasma. *J. Appl. Phys.* **2003**, *94*, 1969–1974.
180. Mangolini, L.; Thimsen, E.; Kortshagen, U. High-Yield Plasma Synthesis of Luminescent Silicon Nanocrystals. *Nano Lett.* **2005**, *5*, 655–659.
181. Bapat, A.; Gatti, M.; Ding, Y.-P.; Campbell, S.A.; Kortshagen, U. A plasma process for the synthesis of cubic-shaped silicon nanocrystals for nanoelectronic devices. *J. Phys. D* **2007**, *40*, 2247–2257.
182. Kendrick, C.; Klafehn, G.; Guan, T.; Anderson, I.; Shen, H.; Redwing, J.; Collins, R. Controlled growth of SiNPs by plasma synthesis. *Sol. Energy Mater. Sol. Cells* **2014**, *124*, 1–9.
183. Cernetti, P.; Gresback, R.; Campbell, S.A.; Kortshagen, U. Nonthermal Plasma Synthesis of Faceted Germanium Nanocrystals. *Chem. Vap. Depos.* **2007**, *13*, 345–350.
184. Gresback, R.; Holman, Z.; Kortshagen, U. Nonthermal plasma synthesis of size-controlled, monodisperse, freestanding germanium nanocrystals. *Appl. Phys. Lett.* **2007**, *91*, 093119.
185. Pi, X.D.; Kortshagen, U. Nonthermal plasma synthesized freestanding silicon-germanium alloy nanocrystals. *Nanotechnology* **2009**, *20*, 295602.
186. Hitzbleck, K.; Wiggers, H.; Roth, P. Controlled formation and size-selected deposition of indium nanoparticles from a microwave flow reactor on semiconductor surfaces. *Appl. Phys. Lett.* **2005**, *87*, 093105.
187. Chau, J.L.H.; Yang, C.-C.; Shih, H.-H. Microwave Plasma Production of Metal Nanopowders. *Inorganics* **2014**, *2*, 278–290.
188. Chau, J.L.H.; Hsu, M.-K.; Hsieh, C.-C.; Kao, C.-C. Microwave plasma synthesis of silver nanopowders. *Mater. Lett.* **2005**, *59*, 905–908.
189. Lee, S.H.; Oh, S.-M.; Park, D.-W. Preparation of silver nanopowder by thermal plasma. *Mater. Sci. Eng. C* **2007**, *27*, 1286–1290.
190. Chau, J.L.H.; Hsu, M.-K.; Kao, C.-C. Microwave plasma synthesis of Co and SiC-coated Co nanopowders. *Mater. Lett.* **2006**, *60*, 947–951.
191. Chau, J.L.H. Synthesis of Ni and bimetallic FeNi nanopowders by microwave plasma method. *Mater. Lett.* **2007**, *61*, 2753–2756.
192. Yasar-Inceoglu, O.; Mangolini, L. Characterization of Si-Ge alloy nanocrystals produced in a non-thermal plasma reactor. *Mater. Lett.* **2013**, *101*, 76–79.
193. Scott, J.H.J.; Turgut, Z.; Chowdary, K.; McHenry, M.E.; Majetich, S.A. Thermal plasma synthesis of Fe-Co alloy nanoparticles. *Mat. Res. Soc. Symp. Proc.* **1998**, *501*, 121–126.
194. Vollath, D.; Szabó, D.V.; Fuchs, J. Polymer coated nanoparticulate ferrite powders: Properties and application. *Mat. Res. Soc. Symp. Proc.* **1999**, *557*, 443–448.
195. Szabó, D.V.; Lamparth, I.; Vollath, D. Complex high frequency properties of ceramic-polymer nanocomposites: Comparison of fluoro-polymers and acrylic-based compounds. *Macromol. Symp.* **2002**, *181*, 393–398.
196. Lamparth, I.; Szabó, D.V.; Vollath, D. Ceramic nanoparticles coated with polymers based on acrylic derivatives. *Macromol. Symp.* **2002**, *181*, 107–112.
197. Vollath, D.; Szabó, D.V.; Schlabach, S. Oxide/polymer nanocomposites as new luminescent materials. *J. Nanopart. Res.* **2004**, *6*, 181–191.

198. Vollath, D.; Szabó, D.V. Synthesis and properties of nanocomposites. *Adv. Eng. Mater.* **2004**, *6*, 117–127.
199. Szabó, D.V.; Reuter, H.; Schlabach, S.; Lellig, C.; Vollath, D. Influence of halides on the luminescence of oxide/antracene/polymer nanocomposites. *Mat. Res. Soc. Symp. Proc.* **2005**, *846*, 77–182.
200. Fuchs, M.; Breitenstein, D.; Fartmann, M.; Grehl, T.; Kayser, S.; Koester, R.; Ochs, R.; Schlabach, S.; Szabó, D.V.; Bruns, M. Characterization of core/shell nanoparticle thin films for gas analytical applications. *Surf. Interface Anal.* **2010**, *42*, 1131–1134.
201. Sagmeister, M.; Brossmann, U.; List, E.; Ochs, R.; Szabó, D.V.; Saf, R.; Grogger, W.; Tchernychova, E.; Würschum, R. Synthesis and optical properties of organic semiconductor/zirconia nanocomposites. *J. Nanopart. Res.* **2010**, *12*, 2541–2551.
202. Vollath, D. Bifunctional nanocomposites with magnetic and luminescence properties. *Adv. Mater.* **2010**, *22*, 4410–4415.
203. Vollath, D.; Szabó, D.V. Synthesis of coated nanoparticulate ceramic powders. *Mat. Res. Soc. Symp. Proc.* **1998**, *520*, 43–148.
204. Chau, J.L.H.; Yang, C.C. Surface modification of silica nanopowders in microwave plasma. *J. Exp. Nanosci.* **2014**, *9*, 357–361.
205. Panchal, V.; Neergat, M.; Bhandarkar, U. Synthesis and characterization of carbon coated nanoparticles produced by a continuous low-pressure plasma process. *J. Nanopart. Res.* **2011**, *13*, 3825–3833.
206. Kim, J.H.; Hong, Y.C.; Uhm, H.S. Binary oxide material made from a mixture of Zn and Cd in a microwave plasma. *Chem. Phys. Lett.* **2007**, *443*, 122–126.
207. Gupta, A.; Schulz, C.; Wiggers, H. Influence of etching and surface functionalization on the optical property of luminescing phosphorus doped silicon nanoparticles. *J. Optoelectron. Adv. Mater.* **2010**, *12*, 518–522.
208. Cho, S.C.; Uhm, H.S.; Bang, C.U.; Lee, D.K.; Han, C.S. Production of nanocrystalline Y<sub>2</sub>O<sub>3</sub>:Eu powder by microwave plasma-torch and its characterization. *Thin Solid Films* **2009**, *517*, 4052–4055.
209. Sato, T.; Suzuki, H.; Kido, O.; Kurumada, M.; Kamitsuji, K.; Kimura, Y.; Kawasaki, H.; Kaneko, S.; Saito, Y.; Kaito, C. Production of transition metal-doped ZnO nanoparticles by using RF plasma field. *J. Cryst. Growth* **2005**, *275*, e983–e987.
210. Wang, X.H.; Li, J.G.; Kamiyama, H.; Katada, M.; Ohashi, N.; Moriyoshi, Y.; Ishigaki, T. Pyrogenic Iron(III)-Doped TiO<sub>2</sub> Nanopowders Synthesized in RF Thermal Plasma: Phase Formation, Defect Structure, Band Gap, and Magnetic Properties. *J. Am. Chem. Soc.* **2005**, *127*, 10982–10990.
211. Li, J.-G.; Wang, X.-H.; Kamiyama, H.; Ishigaki, T.; Sekiguchi, T. RF plasma processing of Er-doped TiO<sub>2</sub> luminescent nanoparticles. *Thin Solid Films* **2006**, *506–507*, 292–296.
212. Li, J.-G.; Büchel, R.; Isobe, M.; Mori, T.; Ishigaki, T. Cobalt-Doped TiO<sub>2</sub> Nanocrystallites: Radio-Frequency Thermal Plasma Processing, Phase Structure, and Magnetic Properties. *J. Phys. Chem. C* **2009**, *113*, 8009–8015.
213. Jung, D.-W.; Park, D.-W. Synthesis of nano-sized antimony-doped tin oxide (ATO) particles using a DC arc plasma jet. *Appl. Surf. Sci.* **2009**, *255*, 5409–5413.

214. Kilibarda, G.; Schlabach, S.; Winkler, V.; Bruns, M.; Hanemann, T.; Szabó, D.V. Electrochemical performance of Tin-based nano-composite electrodes using a vinylene carbonate-containing electrolyte for Li-ion cells. *J. Power Sources* **2014**, *263*, 145–153.
215. Luhrs, C.; Phillips, J.; Fanson, P.T. Production of complex cerium-Aluminum oxides using an atmospheric pressure plasma torch. *Langmuir* **2007**, *23*, 7055–7064.
216. Choi, S.; Lee, M.-S.; Park, D.-W. Photocatalytic performance of TiO<sub>2</sub>/V<sub>2</sub>O<sub>5</sub> nanocomposite powder prepared by DC arc plasma. *Curr. Appl. Phys.* **2014**, *14*, 433–438.
217. Néel, L. Some theoretical aspects on rock-magnetism. *Adv. Phys.* **1955**, *4*, 191–243.
218. Néel, L. Influence des fluctuations thermiques sur l'aimantation de grains ferromagnétiques très fins. *C. R. Hébd. Acad. Sci.* **1949**, *228*, 664–666 (In French).
219. Tang, Z.X.; Sorensen, C.M.; Klabunde, K.J.; Hadjipanayis, G.C. Size-Dependent Magnetic Properties of Manganese Ferrite Fine Particles. *J. Appl. Phys.* **1991**, *69*, 5279–5281.
220. Han, D.H.; Wang, J.P.; Luo, H.L. Crystallite Size Effect on Saturation Magnetization of Fine Ferrimagnetic Particles. *J. Magn. Magn. Mat.* **1994**, *136*, 176–182.
221. Chen, Q.; Zhang, Z.J. Size-dependent superparamagnetic properties of MgFe<sub>2</sub>O<sub>4</sub> spinel ferrite nanocrystallites. *Appl. Phys. Lett.* **1998**, *73*, 3156–3158.
222. Morales, M.P.; Veintemillas-Verdaguer, S.; Serna, C.J. Magnetic properties of uniform  $\gamma$ -Fe<sub>2</sub>O<sub>3</sub> nanoparticles smaller than 5 nm prepared by laser pyrolysis. *J. Mater. Res.* **1999**, *14*, 3066–3072.
223. Batlle, X.; Labarta, A. Finite-size effects in fine particles: magnetic and transport properties. *J. Phys. D* **2002**, *35*, R15–R42.
224. Goya, G.F.; Leite, E.R. Ferrimagnetism and spin canting of Zn<sup>57</sup>Fe<sub>2</sub>O<sub>4</sub> nanoparticles embedded in ZnO matrix. *J. Phys.* **2003**, *15*, 641–651.
225. Witvrouwen, T.; Paulussen, S.; Sels, B. The Use of Non-Equilibrium Plasmas for the Synthesis of Heterogeneous Catalysts. *Plasma Process. Polym.* **2012**, *9*, 750–760.
226. Sun, S.-N.; Wei, C.; Zhu, Z.-Z.; Hou, Y.-L.; Subbu, S.V.; Xu, Z.-C. Magnetic iron oxide nanoparticles: Synthesis and surface coating techniques for biomedical applications. *Chin. Phys. B* **2014**, *23*, 037503.
227. de Montferrand, C.; Lalatonne, Y.; Bonnin, D.; Lièvre, N.; Lecouvey, M.; Monod, P.; Russier, V.; Motte, L. Size-Dependent Nonlinear Weak-Field Magnetic Behavior of Maghemite Nanoparticles. *Small* **2012**, *8*, 1945–1956.
228. Kingery, W.D.; Bowen, H.K.; Uhlmann, D.R. *Introduction to Ceramics*, 2nd ed.; John Wiley & Sons: New York, NY, USA, 1976.
229. Lakowicz, J.R. *Principles of Fluorescence Spectroscopy*, 2nd ed.; Kluwer Academic Press/Plenum Publishers: New York, NY, USA, 1999.
230. Millers, D.; Grigorjeva, L.; Lojkowski, W.; Opalinska, A. Luminescence of ZrO<sub>2</sub> Nanocrystals. *Solid State Phenom.* **2005**, *106*, 103–108.
231. Chen, H.; Wu, X.; Xiong, S.; Zhang, W.; Zhu, J. Red photoluminescence mechanism in SnO<sub>2</sub> nanostructures. *Appl. Phys. A* **2009**, *97*, 365–368.
232. Yang, Y.; Leppert, V.J.; Risbud, S.H.; Twamley, B.; Power, P.P.; Lee, H.W.H. Blue luminescence from amorphous GaN nanoparticles synthesized *in situ* in a polymer. *Appl. Phys. Lett.* **1999**, *74*, 2262–2264.

233. Nienhaus, H.; Kravets, V.; Koutouzov, S.; Meier, C.; Lorke, A.; Wiggers, H.; Kennedy, M.K.; Kruis, F.E. Quantum size effect of valence band plasmon energies in Si and SnO<sub>x</sub> nanoparticles. *J. Vac. Sci. Technol. B* **2006**, *24*, 1156–1161.
234. Zhou, J.; Wang, Y.; Zhao, F.; Wang, Y.; Zhang, Y.; Yang, L. Photoluminescence of ZnO nanoparticles prepared by a novel gel-template combustion process. *J. Lumines.* **2006**, *119–120*, 248–252.
235. Corr, S.A.; O’Byrne, A.; Gun’ko, Y.K.; Ghosh, S.; Brougham, D.F.; Mitchell, S.; Volkov, Y.; Prina-Mello, A. Magnetic-fluorescent nanocomposites for biomedical multitasking. *Chem. Commun.* **2006**, 4474–4476.
236. Chen, D.; Jiang, M.; Li, N.; Gu, H.; Xu, Q.; Ge, J.; Xia, X.; Lu, J. Modification of magnetic silica/iron oxide nanocomposites with fluorescent polymethacrylic acid for cancer targeting and drug delivery. *J. Mater. Chem.* **2010**, *20*, 6422–6429.
237. Gu, Z.; Chen, X.-Y.; Shen, Q.-D.; Ge, H.-X.; Xu, H.-H. Hybrid nanocomposites of semiconductor nanoparticles and conjugated polyelectrolytes and their application as fluorescence biosensors. *Polymer* **2010**, *51*, 902–907.
238. Cho, H.-S.; Dong, Z.; Pauletti, G.M.; Zhang, J.; Xu, H.; Gu, H.; Wang, L.; Ewing, R.C.; Huth, C.; Wang, F.; *et al.* Fluorescent, Superparamagnetic Nanospheres for Drug Storage, Targeting, and Imaging: A Multifunctional Nanocarrier System for Cancer Diagnosis and Treatment. *ACS Nano* **2010**, *4*, 5398–5404.
239. Di Corato, R.; Bigall, N.C.; Ragusa, A.; Dorfs, D.; Genovese, A.; Marotta, R.; Manna, L.; Pellegrino, T. Multifunctional Nanobeads Based on Quantum Dots and Magnetic Nanoparticles: Synthesis and Cancer Cell Targeting and Sorting. *ACS Nano* **2011**, *5*, 1109–1121.
240. Winter, M.; Besenhard, J.O. Electrochemical lithiation of tin and tin-based intermetallics and composites. *Electrochim. Acta* **1999**, *45*, 31–50.
241. Bruce, P.G.; Scrosati, B.; Tarascon, J.M. Nanomaterials for rechargeable lithium batteries. *Angew. Chem. Int. Ed.* **2008**, *47*, 2930–2946.
242. Kilibarda, G.; Schlabach, S.; Hanemann, T.; Szabó, D.V. Influence of Environmental Temperature on the Electrochemical Performance of a Tin-Based Nano-Electrode in Lithium Ion Cells. *Int. J. Electrochem. Sci.* **2013**, *8*, 6212–6219.
243. Kilibarda, G.; Szabó, D.V.; Schlabach, S.; Winkler, V.; Bruns, M.; Hanemann, T. Investigation of the degradation of SnO<sub>2</sub> electrodes for use in Li-ion cells. *J. Power Sources* **2013**, *233*, 139–147.
244. Kilibarda, G. Nanopartikel als Anodenmaterialien: Entwicklung von nanoskaligen Schichtstrukturen auf der Basis von Zinn und Kohlenwasserstoffen für die Anwendung als Anodenmaterial in Li-Ionen-Zellen. PhD Thesis, University Freiburg, Germany, June 2014 (In German).
245. Sato, K.; Noguchi, M.; Demachi, A.; Oki, N.; Endo, M. A Mechanism of Lithium Storage in Disordered Carbons. *Science* **1994**, *264*, 556–558.
246. Dahn, J.R.; Zheng, T.; Liu, Y.; Xue, J.S. Mechanisms for Lithium Insertion in Carbonaceous Materials. *Science* **1995**, *270*, 590–593.
247. Zheng, T.; Liu, Y.; Fuller, E.W.; Tseng, S.; von Sacken, U.; Dahn, J.R. Lithium Insertion in High Capacity Carbonaceous Materials. *J. Electrochem. Soc.* **1995**, *142*, 2581–2590.

248. Liu, Y.; Xue, J.S.; Zheng, T.; Dahn, J.R. Mechanism of lithium insertion in hard carbons prepared by pyrolysis of epoxy resins. *Carbon* **1996**, *34*, 193–200.

© 2014 by the authors; licensee MDPI, Basel, Switzerland. This article is an open access article distributed under the terms and conditions of the Creative Commons Attribution license (<http://creativecommons.org/licenses/by/3.0/>).